

Thank you very much for pointing out several issues with the most recent version of our manuscript. We noticed a few others as well in our final read through. Below, we've included a summary of the changes made to this version of the manuscript.

Line 31: Replace "sync" with "synchrony." Replaced "brief" with "millennial-scale."

Line 32: Replaced "an" with "a."

Line 88: Added "history."

Lines 258-261: updated dates in Mineralogy section.

Lines 282 -284: Shortened genus names for genera already mentioned.

Line 289: Removed extra paragraph marker and typos.

Line 290: Replaced "and these optima" with "that."

Lines 328-329: updated eponitic diatoms results after transfer of several species out of this niche.

Lines 510-511: changed description of sea ice reduction to reflect new information from eponitic species.

Line 617: Changed "tantalizing" to "possible"

Line 700: updated mineralogy date.

Line 843: included data archive web address.

Table 3: Species names updated in several places.

The following references that only appear in figure captions were added to the list of references: Barr and Clark, 2009; Cavalieri, et al., 1996; Gualtieri, et al., 2000; Heiser and Roush, 2001; Kaufman et al., 2011; Kim et al., 2015; Manley, 2002; Meyers, 1994; Redfield, 1963; and Walinsky, et al., 2009.

Figure 7: Changed cells/g to calcareous nannofossils/gram in figure and in caption. Revised eponitic diatom plot in light of change in species niche in Table 3.

1 **Bering Sea surface water conditions during Marine**
2 **Isotope Stages 12 to 10 at Navarin Canyon (IODP Site**
3 **U1345)**

4

5 **Beth E. Caissie¹, Julie Brigham-Grette², Mea S. Cook³, Elena Colmenero-**
6 **Hidalgo⁴**

7 [1]{Iowa State University, Ames, Iowa}

8 [2]{University of Massachusetts, Amherst, Amherst, Massachusetts}

9 [3]{Williams College, Williamstown, Massachusetts}

10 [4]{Universidad de León, León, Spain}

11 Correspondence to: B.E. Caissie (bethc@iastate.edu)

12

13 **Abstract**

14 Records of past warm periods are essential for understanding interglacial climate system
15 dynamics. Marine Isotope Stage 11 occurred 425-394 ka when global ice volume was the
16 lowest, sea level was the highest and terrestrial temperatures were the warmest of the last
17 500 kyrs. Because of its extreme character, this interval has been considered an analog
18 for the next century of climate change. The Bering Sea is ideally situated to record how
19 opening or closing of the Pacific-Arctic Ocean gateway (Bering Strait) impacted primary
20 productivity, sea ice, and sediment transport in the past; however, little is known about
21 this region prior to 125 ka. IODP Expedition 323 to the Bering Sea offered the
22 unparalleled opportunity to look in detail at time periods older than had been previously
23 retrieved using gravity and piston cores. Here we present a multi-proxy record for Marine
24 Isotope Stages 12-10 from Site U1345 located near the continental shelf-slope break.
25 MIS 11 is bracketed by highly productive laminated intervals that may have been
26 triggered by flooding of the Beringian shelf. Although sea ice is reduced during the early
27 MIS 11 laminations, it remains present at the site throughout both glacial and MIS 11.

28 High summer insolation is associated with higher productivity, but colder SSTs, which
29 implies that productivity was likely driven by increased upwelling. Multiple examples of
30 Pacific-Atlantic teleconnections are presented including laminations deposited at the end
31 of MIS 11 in synchrony with millennial-scale expansions in sea ice in the Bering Sea and
32 stadial events seen in the North Atlantic. When global eustatic sea level was at its peak, a
33 series of anomalous conditions are seen at U1345. We examine whether this is evidence
34 for a reversal of Bering Strait Through Flow, an advance of Beringian tidewater glaciers,
35 or a turbidite.

36

37 **1 Introduction**

38 Predictions and modeling of future climate change require a detailed understanding of
39 how the climate system works. Reconstructions of previous warm intervals shed light on
40 interhemispheric teleconnections. The most recent interglacial period with orbital
41 conditions similar to today was approximately 400 ka, during the extremely long
42 interglacial known as Marine Isotope Stage (MIS) 11. CO₂ concentration averaged
43 approximately 275 ppm, which is similar to pre-industrial levels (EPICA Community
44 Members, 2004). The transition from MIS 12 into MIS 11 has been compared to the last
45 deglaciation (Dickson et al., 2009) and extreme warmth during MIS 11 has been
46 considered an analog for future warmth (Droxler et al., 2003; Loutre and Berger, 2003),
47 although the natural course of interglacial warmth today has been disrupted by
48 anthropogenic forcing (IPCC, 2013).

49 Despite the work done to characterize the warmth of MIS 11 in the terrestrial realm
50 (Candy et al., 2014; Melles et al., 2012; Prokopenko et al., 2010), as well as the North
51 Atlantic (Bauch et al., 2000; Chaisson et al., 2002; Dickson et al., 2009; Milker et al.,
52 2013; Poli et al., 2010), little is known about this interval from the North Pacific and
53 Bering Sea region (Candy et al., 2014). Modeling studies describe several mechanisms
54 for linking the Atlantic and Pacific through oceanic heat transport on glacial-interglacial
55 time scales (DeBoer and Nof, 2004; Hu et al., 2010), however, there have been no tests of
56 these modeling studies using proxy data older than 30 ka. Furthermore, the location of the
57 Bering Sea marginal sea ice zone advanced and retreated hundreds of kilometers during

Beth Caissie 8/4/2016 1:51 PM

Deleted: brief

Beth Caissie 8/4/2016 1:30 PM

Deleted: n

60 the past three glacial-interglacial cycles (Caissie et al., 2010; Katsuki and Takahashi,
61 2005; Sancetta and Robinson, 1983); however, sea surface and intermediate water
62 variability before MIS 5 is unknown.

63 This investigation of terrestrial-marine coupling at the shelf-slope break from MIS 12 to
64 10 is the first study of this interval in the subarctic Pacific (Fig. 1). We use a multi-proxy
65 approach to examine orbital- and millennial-scale changes in productivity and sea ice
66 extent. We demonstrate that insolation plays a major role in these changes, but that sea
67 ice also shows rapid, millennial-scale variability. Finally, we test the hypotheses that 1) in
68 Beringia, tidewater glaciers advanced while sea level was high and 2) Bering Strait
69 Through Flow reversed shortly after the MIS 12 glacial termination (Termination V). We
70 find inconclusive evidence of a glacial advance, but no evidence of Bering Strait reversal.

71

72 **2 Background**

73 **2.1 Global and Beringian Sea Level during MIS 11**

74 The maximum height of sea level during MIS 11 is an open question with estimates
75 ranging from 6 to 13 m above present sea level (apsl) (Dutton et al., 2015) to 0 m apsl
76 (Rohling et al., 2010; Rohling et al., 2014). The discrepancy may stem from large
77 differences between global eustatic (Bowen, 2010) or ice-volume averages (McManus et
78 al., 2003) and regional geomorphological or micropaleontological evidence (van
79 Hengstum et al., 2009). Regional isostatic adjustment due to glacial loading and
80 unloading are now known to be significant and regional highstands may record higher
81 than expected sea levels if glacial isostasy and dynamic topography have not been
82 accounted for, even in places that were never glaciated (PAGES et al., 2016; Raymo and
83 Mitrovica, 2012; Raymo et al., 2011). For example, Raymo and Mitrovica (2012) suggest
84 eustatic sea level during MIS 11 was 6-13 m apsl globally and near 5 m apsl locally in
85 Beringia, yet MIS 11 shorelines are at +22 m today in northwest Alaska (Kaufman and
86 Brigham-Grette, 1993) due to this complex geophysics.

87 Regardless of the ultimate height of sea level, the transition from MIS 12 to MIS 11
88 records the greatest change in sea level of the last 500 ka (Rohling et al., 2014); sea level

89 rose from perhaps -140 m to its present level or higher (Bowen, 2010)(Dutton et al.,
90 | 2015). Sea level [history](#) during MIS 11 may have been complex (Kindler and Hearty,
91 2000), but most records agree that sea level during this exceptionally long interglacial (30
92 kyrs) was highest from 410 to 401 ka, coincident with a second peak in June insolation at
93 65°N. This long highstand most likely requires partial or complete collapse of the
94 Greenland ice sheet (up to 6 m) (de Vernal and Hillaire-Marcel, 2008; Reyes et al., 2014)
95 and/or the West Antarctic Ice Sheet (Scherer et al., 1998), but not the East Antarctic Ice
96 Sheet (Berger et al., 2015; Dutton et al., 2015; Raymo and Mitrovica, 2012). It has
97 frequently been hypothesized that the West Antarctic Ice Sheet collapsed during MIS 11
98 and modeling studies confirm this (Pollard and DeConto, 2009), however unconformities
99 in the record prevent confirmation of a collapse (McKay et al., 2012). Yet, Teitler (2015)
100 show that IRD during MIS 11 dropped as low as it was during MIS 31, when it is clear
101 that the West Antarctic Ice Sheet had collapsed (Naish et al., 2009). With uncertainties,
102 East Antarctica ice was stable; however, small changes in either sector of the Antarctic
103 ice sheet may have contributed up to 5 m of sea level rise (Berger et al., 2015; EPICA
104 Community Members, 2004).

105 The sea level history of Beringia defines Arctic communication between the Pacific and
106 the Atlantic oceans during the Plio-Pleistocene. As a region, Beringia consists of both the
107 terrestrial and marine regions north of the Aleutian Islands that stretch to the shelf-slope
108 break in the Bering, East Siberian, Chukchi, and Beaufort seas (Fig. 1). On land, Beringia
109 extends from the Lena River in Siberia to the Mackenzie River in Canada. Large portions
110 of the Beringian shelf were exposed when sea level dropped below -50 m (Hopkins,
111 1959) and this subaerial expanse stretches more than 1000 km from north to south during
112 most glacial periods (Fig. 2). In contrast, as sea level rises at glacial terminations the
113 expansive continental shelf is flooded, rapidly once sea level reaches -60 mpsl (Keigwin
114 et al., 2006). This introduces fresh organic matter and nutrients into the southern Bering
115 Sea (i.e. Bertrand et al., 2000; Shiga and Koizumi, 2000; Ternois et al., 2001), re-
116 establishing at -50 mpsl the connection between the Pacific and Atlantic oceans through
117 Bering Strait (Keigwin et al., 2006). The late Cenozoic history of the depth of the Bering
118 Strait sill is poorly known, hence current oceanographic reconstructions (e.g., Knudson
119 and Ravelo, 2015) assume that a sill depth of -50 mpsl was temporally stable, which is

120 probably not the case and requires future study. However, in this study, we also assume
121 that a sill depth of -50 mpsl controls oceanographic communication between the Atlantic
122 and Pacific Oceans.

123

124 **2.2 Site Location and Oceanographic Setting**

125 The Integrated Ocean Drilling Program's (IODP) Expedition 323, Site U1345, is located
126 on an interfluvial ridge near the shelf-slope break in the Bering Sea (Fig. 1). Navarin
127 Canyon, one of the largest submarine canyons in the world (Normack and Carlson, 2003)
128 is located just to the northwest of the site. Sediments were retrieved from ~1008 m of
129 water, placing the site within the center of the modern day oxygen minimum zone
130 (Takahashi et al., 2011). We focus on this site because of its proximity to the modern
131 marginal ice zone in the Bering Sea and observed high sedimentation rates. Its siting on
132 top of an interfluvial ridge was chosen to reduce the influence of turbidites moving through
133 Navarin Canyon.

134 Today, water circulates cyclonically in the deep basins of the Bering Sea (Fig. 1). Site
135 U1345 is influenced by the northwest flowing Bering Slope Current (BSC), which is
136 derived from the Alaskan Stream (AS). South of the Aleutian Islands, the Alaskan
137 Stream flows westward and enters the Bering Sea through deep channels in the western
138 Aleutian Islands. Once north of the Aleutian Islands, this water mass becomes the
139 Aleutian North Slope Current (ANS), and flows eastward until it reaches the Bering Sea
140 shelf. Interactions with the shelf turn this current to the northwest where it becomes the
141 Bering Slope Current (Stabeno et al., 1999). Tidal forces and eddies in the Bering Slope
142 Current drive upwelling through Navarin Canyon and other interfluvial ridges along the shelf-
143 slope break (Kowalik, 1999). The resulting cold water and nutrients brought to the sea
144 surface, coupled with the presence of seasonal sea ice, drive the high productivity found
145 today in the so called "Green Belt" (Springer et al., 1996) along the shelf-slope break.
146 North of the site, low salinity, high nutrient shelf waters (Cooper et al., 1997) primarily
147 flow north through the Bering Strait to the Arctic Basin (Schumacher and Stabeno, 1998).

148

149 **3 Methods**

150 **3.1 Age Model**

151 The age model (Fig. 3) is derived from the shipboard age model, which was developed
152 using magnetostratigraphy and biostratigraphy. First and last appearance datums for
153 diatoms and radiolarians make up the majority of the biostratigraphic markers used to
154 place the record in the correct general stratigraphic position (Takahashi et al., 2011).
155 Oxygen isotope measurements taken on the benthic foraminifera, *Uvigerina peregrina*,
156 *Nonionella labradorica*, and *Globobulimina affinis* (Cook et al., 2016) were then used to
157 tune site U1345 to the global marine benthic foraminiferal isotope stack (LR04) (Lisiecki
158 and Raymo, 2005) (Fig. 3; Table 1). Based on this combined age model, MIS 11 spans
159 from 115.3 to 130.6 mbsf (Cook et al., 2016); however, the characteristic interglacial
160 isotopic depletion was not found in U1345 which means that the exact timing of peak
161 interglacial conditions is unknown.

162 The nearby core, IODP Exp 323, Site U1343 (Fig. 1) has an excellent oxygen isotopic
163 record during MIS 11 (Asahi et al., 2016). We compared the two isotopic records and
164 their magnetic susceptibilities (Fig. 3) and found that even with only two tie points, there
165 was good correlation between the timing of the onset of laminated intervals and also the
166 interglacial increase in magnetic susceptibility (Fig. 3b). We added one additional tie
167 point to connect the inflection points in magnetic susceptibility (Table 1). In U1343, this
168 point occurred at 398.50 ka. U1345 was shifted 1.5 ka younger in order to align with
169 U1343. The addition of this point allows us to have more confidence in the timing of
170 peak interglacial conditions in U1345. However, given the oxygen isotope sampling
171 resolution, as well as the stated error in the LR04 dataset (4 kyr), we estimate the error of
172 the age model could be up to 5 kyr. Therefore, we urge caution when comparing
173 millennial scale changes at this site with other sites that examine MIS 11 at millennial
174 scale resolution or finer.

175 Sedimentation rates during the study interval range from 29 cm/kyrs to 45 cm/kyr with
176 the highest sedimentation rates occurring during glacial periods. Depths and ages of
177 major climate intervals referred to in the text are found in Table 2.

178

179 **3.2 Sediment Analyses**

180 Details about sediment sampling can be found in the Supplementary Materials.
181 Quantitative diatom slides were prepared (Scherer) and counted (Schrader and Gersonde,
182 1978) using published taxonomic descriptions and images (Hasle and Heimdal, 1968;
183 Koizumi, 1973; Lundholm and Hasle, 2008, 2010; Medlin and Hasle, 1990; Medlin and
184 Priddle, 1990; Onodera and Takahashi, 2007; Sancetta, 1982, 1987; Syvertsen, 1979;
185 Tomas, 1996; Witkowski et al., 2000). Diatom taxa were then grouped according to
186 ecological niche (Table 3) based on biological observations (Aizawa et al., 2005; Fryxell
187 and Hasle, 1972; Håkansson, 2002; Horner, 1985; Saito and Taniguchi, 1978;
188 Schandelmeier and Alexander, 1981; von Quillfeldt, 2001; von Quillfeldt et al., 2003)
189 and statistical associations (Barron et al., 2009; Caissie et al., 2010; Hay et al., 2007;
190 Katsuki and Takahashi, 2005; Lopes et al., 2006; McQuoid and Hobson, 2001; Sancetta,
191 1982, 1981; Sancetta and Robinson, 1983; Sancetta and Silvestri, 1986; Shiga and
192 Koizumi, 2000). In cases where a diatom species was reported to fit into more than one
193 environmental niche, it was grouped into the niche where it was most commonly
194 recognized in the literature.

195 Eighteen quantitative calcareous nannofossil slides were prepared (Flores and Sierro,
196 1997) and counted using a Zeiss polarized light microscope at 1000x magnification.
197 Samples were considered barren if no coccoliths were found in at least 165 randomly
198 selected fields of view. All taxa were identified to the species or variety level (Flores et
199 al., 1999; Young et al., 2003).

200 Grain size of both biogenic and terrigenous sediment was measured using a Malvern
201 Mastersizer 3000 with the Hydro MV automated wet dispersion unit. The mineralogy of
202 ten samples was analyzed using a Siemens D-5000 X-Ray Diffractometer (Eberl, 2003)

203 The carbon and nitrogen isotopic and elemental composition of organic matter was
204 determined by Dumas combustion using a Carlo Erba 1108 elemental analyzer coupled to
205 a Thermo-Finnigan Delta Plus XP isotope ratio mass spectrometer at the University of
206 California Santa Cruz Stable Isotope Laboratory. The 1-sigma precision of stable isotope
207 measurements and elemental composition of carbon are 0.2‰ and 0.03%, respectively,
208 and for nitrogen are 0.2‰ and 0.002‰, respectively. $\delta^{13}\text{C}$ values are reported relative to

209 the Vienna Pee Dee Belemnite (VPDB) and $\delta^{15}\text{N}$ values are reported relative to
210 atmospheric N_2 . Percent CaCO_3 was calculated according to Schubert and Calvert (2001).
211 More detailed methodology can be found in the Supplemental Materials.

212

213 **4 Results**

214 **4.1 Sedimentology**

215 The sediments at Site U1345 are massive with centimeter-scale dark or coarse-grained
216 mottles. They are mainly composed of clay and silt with varying amounts of diatoms,
217 sand, and tephra throughout. Laminated intervals bracket MIS 11 (Fig. 4). The proportion
218 of diatoms relative to terrigenous or volcanogenic grains is highest during laminated
219 intervals and lowest immediately preceding Termination V (~425 ka). Vesiculated tephra
220 shards were seen in every diatom slide analyzed. Several thin (< 1 cm) sand layers and
221 shell fragments were visible on the split cores, especially during MIS 12. However, high-
222 resolution grain size analyses show that the median grain size was lowest during MIS 12,
223 increasing from approximately 14 μm to 21 μm at the start of Termination V at 424.5 ka
224 (130.92 mbsf). Median grain size peaks at 84 μm between 401 and 407 ka (125.42-
225 123.62 mbsf). This interval is also the location of an obvious sandy layer in the core.
226 After this “anomalous interval,” median grain size remains steady at about 17 μm .
227 Subrounded to rounded clasts (granule to pebble) commonly occur on the split surface of
228 the cores. We combined clast and sand layer data from all Holes at Site U1345 when
229 examining their distribution (Fig. 4).

230 A 3.5 m thick laminated interval, estimated to span 12 kyrs (see Table 4 for depths and
231 ages) is deposited beginning during Termination V. Although the termination is short-
232 lived and the laminated interval quite long, we refer to it as the Termination V
233 Laminations for the sake of clarity throughout this manuscript. The next laminated
234 interval occurs at about 394 ka and lasts approximately 1.1 kyrs. During the transition
235 from late MIS 11 to MIS 10, a series of four thin laminated intervals are observed. Each
236 interval lasts between 0.34 and 1.25 ka (Table 4). In general, the upper and lower
237 boundaries of laminated intervals are gradational; however the boundaries between
238 individual lamina are sharp (Takahashi et al., 2011). There are two types of laminations.

239 The Termination V Laminations are Type I laminations: millimeter-scale alternations of
240 black, olive gray, and light brown triplets. In addition to containing a high proportion of
241 diatoms, this type of laminated interval also contains high relative proportions of
242 calcareous nannofossils and foraminifera (Takahashi et al., 2011). The majority of
243 laminations are parallel; however, a 7 cm interval during the Termination V Laminations
244 is highly disturbed in Hole A, showing recumbent folds in the laminations (Takahashi et
245 al., 2011). This interval was not sampled. Type II laminations occur throughout the
246 remainder of MIS 11. These laminations have fewer diatoms and tend to be couplets of
247 siliciclastic sediments with <40% diatoms (Takahashi et al., 2011). Percent CaCO₃ also
248 increases during these laminations though foraminifera and calcareous nannofossils are
249 very rarely seen. None of these later laminated intervals contain any evidence of
250 disturbance.

251 4.2 Mineralogy

252 We determined the weight percent of 23 common minerals in ten samples across the
253 study interval. Samples are primarily composed of quartz, plagioclase, tephra, illite and
254 chlorite with minor amounts of other clay and non-clay minerals (Table 5). Downcore,
255 the largest variability occurs in the weight percent of quartz, chlorite, and illite. In
256 | general, chlorite comprises nearly 35% of the minerals present in the sediments until 399
257 | ka, and then declines ~ 5% for the remainder of MIS 11. Conversely, quartz increases
258 | from 422 to 397 ka and then comprises ~15% of the minerals for the remainder of MIS
259 | 11. Illite is lower than 2% of the mineral assemblage at 424 ka, and then increases rapidly
260 | to nearly 10% at 422 ka. It remains near 10% for the remainder of MIS 11 except for a
261 | brief negative excursion at 397 ka.

262

263 4.3 Diatoms

264 4.3.1 Diatom Assemblages

265 A total of 97 different diatom taxa were identified. Individual samples include between
266 26 and 46 taxa each with an average of 37 taxa. Both types of laminated intervals contain
267 fewer taxa than bioturbated intervals do. This decrease in diversity is confirmed using the

Beth Caissie 8/11/2016 12:22 AM

Deleted: 408

Beth Caissie 8/11/2016 12:24 AM

Deleted: 5

Beth Caissie 8/11/2016 12:24 AM

Deleted: 406

Beth Caissie 8/11/2016 12:24 AM

Deleted: 406

272 Margalef, Simpson, and Shannon indices (Maurer and McGill, 2011) which all show
273 similar down-core profiles (Fig. 5). The Margalef index is a measure of species richness.
274 It shows a decrease in the number of taxa during four out of five laminated intervals that
275 are sufficiently well sampled. Between laminated intervals, there is also a noted decrease
276 in taxa at 388 ka. The Simpson index measures the evenness of the sample. Values close
277 to 1 indicate that all taxa contain an equal number of individuals, while values close to 0
278 indicate that one species dominates the assemblage. In general, the Simpson index is
279 close to 1 throughout the core; however, during the Termination V Laminations and the
280 most recent two laminations, the Simpson index decreases reflecting the dominance by
281 *Chaetoceros* RS during these intervals (Fig. 5). The Simpson index never approaches 0,
282 which would likely indicate a strong dissolution signal. The Shannon diversity index
283 measures both species richness and evenness. Correspondingly, it is low during three of
284 the laminated intervals, high during MIS 12 and peaks at 397 ka (Fig. 5).

285 Absolute diatom abundances vary between 10^6 and 10^8 diatoms deposited per gram of
286 sediment with values an order of magnitude higher during most laminated intervals than
287 during massive intervals (Fig. 5). The diatom assemblage is dominated by *Chaetoceros*
288 and *Thalassiosira antarctica* resting spores (RS), with lesser contributions from
289 *Fragilariopsis oceanica*, *F. cylindrus*, *Fossula arctica*, *Shionodiscus trifultus* (= *T.*
290 *trifulta*), *T. binata*, small (<10 μm in diameter) *T.* species, *Paralia sulcata*, *Lindavia* cf.
291 *ocellata*, *Neodenticula seminae*, and *Thalassionema nitzschioides* (Fig. 6).

292

293 4.3.2 Qualitative Diatom Proxies

294 Diatoms, like many organisms, thrive under a specific range of environmental conditions
295 or optima that are different for each species. For this reason, diatom assemblages are
296 excellent paleoceanographic indicators (Smol, 2002). We grouped diatoms with similar
297 environmental niches together (Table 3) to interpret the paleoceanographic sea surface
298 conditions at the Bering Sea shelf-slope break during MIS 12 to 10 (Caissie, 2012;
299 [Caissie and Nesterovich, In Prep](#); Katsuki and Takahashi, 2005; Sancetta, 1982) (Fig. 7).

300 Grouping diverse species together may result in a loss of information when two different
301 species in the same niche show differing abundance patterns over time. On the other

Beth Caissie 8/4/2016 1:18 PM

Deleted: fragilariopsis

Beth Caissie 8/4/2016 1:18 PM

Deleted: Thalassiosira

Beth Caissie 8/4/2016 1:18 PM

Deleted: Thalassiosira

Beth Caissie 8/4/2016 1:19 PM

Deleted: Thalassiosira

Beth Caissie 8/4/2016 1:11 PM

Deleted: m

... [1]

Beth Caissie 8/4/2016 1:53 PM

Deleted: and these optima

Beth Caissie 8/4/2016 3:04 PM

Deleted: {Caissie and Nesterovich, In Prep}

310 hand, changes in abundances may simply reflect different species filling the same niche
311 at different times.

312 *Chaetoceros* resting spores are the dominant taxa included in the high productivity group
313 (Table 3). Relative percent abundances of *Chaetoceros* RS are highest (up to 69%) during
314 the Termination V Laminations and follow the pattern of both diatom accumulation rate
315 and insolation at 65° N (Berger and Loutre, 1991). The lowest relative abundances (15-
316 20%) of *Chaetoceros*/high productivity species occur between 403 and 390 ka (124.21 to
317 120.07 mbsf) when both obliquity and insolation are low (Fig. 7h).

318 Epontic diatoms are those that bloom attached to the underside of sea ice or within brine
319 channels in the ice (Alexander and Chapman, 1981). This initial bloom occurs below the
320 ice as soon as enough light penetrates to initiate photosynthesis in the Bering Sea, which
321 can occur as early as March (Alexander and Chapman, 1981). A second ice-associated
322 bloom occurs as sea ice begins to break up on the Bering Sea shelf. This bloom is
323 referred to as the marginal ice zone bloom and many of its members are common species
324 in the sediment assemblage. Several diatom species are present in both types of sea ice
325 blooms, and so while they are indicators of ice presence, they cannot be used to
326 distinguish between types of sea ice. These species are grouped under “both ice types”
327 (Table 3).

328 Epontic species are present in very low relative percent abundances (< 1%) throughout
329 much of the record, present only when fresh water diatoms also increase (Fig. 7i, 7n).

330 Marginal ice zone species fluctuate between 4% and 14% throughout the record and do
331 not show any trends in abundance changes (Fig. 7j). The grouping of species found both
332 within the ice and in the water surrounding ice, however, is also somewhat reduced
333 during laminated intervals (Fig. 7k).

334 A cold layer of water found between seasonally warmer surface and warmer deep water
335 characterizes dicothermal water. It is stable because of its very low salinity. In the Sea of
336 Okhotsk and the Bering Sea today, the dicothermal layer is associated with melting sea
337 ice. Genera present in the Bering Sea during late summer tend to co-vary with the
338 dicothermal water indicators, so the two groups were merged for comparison with other
339 diatom groups. *S. trifultus* is the dominant species in the dicothermal group (Table 3). It

Beth Caissie 8/11/2016 12:28 AM

Deleted: 5

Beth Caissie 8/11/2016 12:29 AM

Deleted: but there is a marked absence of them during the laminated interval from 423 to 410 ka (129.96-126.45 mbsf)

344 is relatively high (~4%) during MIS 12, is virtually absent from the sediments during the
345 Termination V Laminations, and then increases again until it peaks at 10% relative
346 abundance at 400 ka (123.22 mbsf) (Fig. 6).

347 Neritic species maintain ~10% relative abundance throughout the core (Fig. 7m). The
348 dominant species in the neritic group is *Paralia sulcata* (Table 3), sometimes considered
349 an indicator of shallow, moving water (Sancetta, 1982). Neritic species are lowest during
350 the Termination V Laminations and increase dramatically around 404 ka (124.61 mbsf)
351 to almost 50% of the assemblage (Fig. 7n). *L. cf. ocellata* is the dominant taxa in the
352 fresh water group. This group is notably absent from much of the core, but prevalent
353 between 401 and 392 ka (123.70 mbsf and 121.20 mbsf); it reaches its highest relative
354 percent abundance (12%) at 401 ka (123.62 mbsf) (Fig. 7n).

355 *Neodenticula seminae* is used here as a tracer of Pacific water (Caissie et al., 2010;
356 Katsuki and Takahashi, 2005). Absolute abundances begin to increase at 422 ka as global
357 eustatic sea level rises above -50 mpsl. Abundance then decreases slowly over the
358 course of the Termination V Laminations and peaks again at 392 ka and 382 ka. As sea
359 level drops below -50 mpsl, *N. seminae* is no longer present at U1345. Relative percent
360 abundances remain stable at ~2% relative percent abundance between 422 and 400 ka
361 (129.62-123.62 mbsf), then peak at 13% at 392 ka (121.22 mbsf) (Fig. 6 and 7o).

362 Diatoms associated with warmer water or classified as members of temperate to
363 subtropical assemblages (Table 3) are quite low throughout the record (<5%), and are
364 highest (3-4%) during mid to late MIS 11 approximately ~410 to 391 ka (126.74 to
365 116.50 mbsf) (Fig. 7p).

366

367 **4.4 Calcareous Nannofossils**

368 Calcareous nannofossils were examined between 432-405 ka (133.4 to 125.0 mbsf); one
369 third of the samples were barren (Fig. 7g, open purple circles) and only one sample (418
370 ka; 128.8 mbsf) had sufficient individuals to estimate relative percent abundances (Fig.
371 7g). This sample is located midway through the Termination V Laminations when the
372 diatom assemblage is overwhelmingly dominated by *Chaetoceros* RS. Small

373 *Gephyrocapsa* dominates (>50%) the calcareous nannofossil assemblage. There are 35%
374 medium *Gephyrocapsa*, 9% *Coccolithus pelagicus*, and 1% *Gephyrocapsa oceanica*.

375

376 **4.5 Geochemistry**

377 **4.5.1 Organic and Inorganic Carbon Content**

378 Total organic carbon (TOC) roughly follows the trend of relative percent abundances of
379 *Chaetoceros* RS, with higher values during the Termination V Laminations (Fig. 7b, 7h).
380 Mean TOC value during MIS 12 is 0.76%, and during the Termination V Laminations, it
381 is 1.11%. TOC decreases between 408 (125.82 mbsf) and 404 ka (124.77 mbsf) coeval
382 with a decrease in $\delta^{15}\text{N}$ values. After 404 ka, it increases linearly to 374 ka (115.39
383 mbsf). TOC is again high during the late MIS 11/MIS 10 laminations.

384 In contrast, inorganic carbon, calculated as % CaCO_3 is less than 1% for most of the
385 record (Fig. 7g). However, it increases up to 3.5% during the laminated intervals and also
386 at 382 ka (117.87 mbsf), 392 ka (110.00 mbsf), and 408 ka (125.82 mbsf).

387

388 **4.5.2 Terrigenous vs. Marine Input Indicators**

389 Nitrogen, carbon and their isotopes can be used to determine relative amounts of
390 terrigenous vs. marine organic mater input. Total nitrogen (TN) is significantly correlated
391 with total organic carbon (TOC) (Fig. 8a); however, the y-intercept of a regression line
392 through the data is 0.03 (Fig. 8a), indicating that there is a significant fraction of
393 inorganic nitrogen in the sediments (Schubert and Calvert, 2001). Inorganic nitrogen can
394 be adsorbed onto clay particles or incorporated into the crystal lattice of potassium-rich
395 clays such as illite. This complicates interpretations of elemental nitrogen and its isotopes
396 because the presence of inorganic nitrogen will lower $\text{C}_{\text{org}}/\text{N}$ ratios and $\delta^{15}\text{N}$ values
397 (Muller, 1977; Schubert and Calvert, 2001).

398 Bearing this bias in mind, the relative terrigenous contribution to the sediments can be
399 estimated by examining where U1345 samples plot in relation to typical $\text{C}_{\text{org}}/\text{N}$, $\delta^{15}\text{N}$, and
400 $\delta^{13}\text{C}$ values for marine phytoplankton, refractory soil organic matter, and C3 vascular
401 plants (Fig. 8). Note that we use $\text{N}/\text{C}_{\text{org}}$, the inverse of $\text{C}_{\text{org}}/\text{N}$, because we seek to derive

402 the terrigenous carbon fraction rather than the fraction of terrigenous nitrogen (Perdue
403 and Koprivnjak, 2007). Throughout MIS 12-10, organic matter is comprised of a mixture
404 of marine and terrigenous organic matter. There is a higher contribution of marine
405 organic matter during MIS 12, 10, and between 394 and 405 ka and a higher contribution
406 of terrigenous organic matter during peak MIS 11 (Fig. 8). The N/C_{org} ratio indicates that
407 during peak MIS 11, this terrigenous organic matter is likely refractory soil organic
408 matter, rather than fresh vascular plant organic matter (Fig. 8b).

409 During MIS 12, C_{org}/N is highly variable, when sea level is below -50 m aspl (Fig. 7). As
410 sea level rises during Termination V, C_{org}/N values increase from 6 to more than 9. The
411 highest C_{org}/N value occurs at the start of the Termination V Laminations. C_{org}/N
412 decreases as sea level rises until at 400 ka (123.62 mbsf) it stabilizes near 7 for the
413 remainder of the record (Fig. 7).

414 Carbon isotopic values range between -22 ‰ and -26 ‰. No sample has low enough $\delta^{13}C$
415 values to be comprised fully of typical Arctic Ocean marine phytoplankton (-22 to -19‰)
416 or ice-related plankton (-18.3‰) (Schubert and Calvert, 2001); however samples from
417 MIS 10, MIS 12, and the “anomalous interval” all plot close to marine phytoplankton
418 values (Fig. 8b). At the onset of the Termination V Laminations, $\delta^{13}C$ becomes more
419 negative and then gradually increases to a maximum of -22.33 at 404 ka (124.62). After
420 400 ka (123.5 mbsf), $\delta^{13}C$ is relatively stable around -23.5‰ (Fig 7).

421

422 **4.5.3 Nitrogen Isotopes**

423 The nitrogen isotopic composition of bulk marine sediments can be thought of as a
424 combination of the $\delta^{15}N$ of the source nitrate and the amount of nitrogen utilization by
425 phytoplankton (Brunelle et al., 2007). Denitrification is common in the low oxygen
426 waters of the eastern tropical North Pacific (Liu et al., 2005) and in the Bering Sea during
427 the Bølling-Allerød (Schlung et al., 2013), leading to enriched core top $\delta^{15}N$ values
428 between 8 and 9‰. When diatoms utilize nitrogen, they preferentially assimilate the
429 lighter isotope, ^{14}N , which enriches surface waters with respect to ^{15}N (Sigman et al.,
430 1999). Complete nitrogen utilization would result in $\delta^{15}N$ values identical to that of the
431 source nitrate (Sigman et al., 1999). Sponge spicules (very low $\delta^{15}N$ values) and

432 radiolarians (highly variable $\delta^{15}\text{N}$ values) may contaminate the $\delta^{15}\text{N}$ of bulk organic
433 matter; therefore, we looked for and found no correlation between spicule abundance and
434 $\delta^{15}\text{N}$ in our samples.

435 $\delta^{15}\text{N}$ is relatively stable, but quite high throughout the study interval, fluctuating around
436 an average value of 6.4‰ and reaching values greater than 7‰ and up to 8‰ several
437 times (Fig. 7). There are several notable excursions from these high values. Coeval with
438 sea level rise and increased relative percent *Chaetoceros* RS, $\delta^{15}\text{N}$ decreased 2.7‰ to
439 4.4‰ before recovering to average values during the Termination V Laminations. Two
440 other depletions occur at 405 ka (124.77 mbsf) and 393 ka (121.62 mbsf), the first is the
441 most extreme and reaches 2.9‰.

442

443 **5 Discussion**

444 **5.1 Orbital-Scale Changes in Productivity and Sea Ice**

445 The observed changes in diatom assemblages and lithology (Fig. 7) allow us to break the
446 sedimentary record into five zones: MIS 12, Termination V, Peak MIS 11, Beringian
447 Glacial Initiation, and Late MIS 11 (Table 2). These zones reflect changing sea ice,
448 glacial ice, sea level, and SST and correspond to events recognized elsewhere in ice cores
449 and marine and lake sediments.

450

451 **5.1.1 Marine Isotope Stage 12 and Early Deglaciation (431-425 ka)**

452 From 431 to 425 ka, the record chronicles conditions at the end of MIS 12. Although
453 diatom accumulation rate is quite low, a relatively diverse assemblage characterizes this
454 period (Fig. 5) with moderate amounts of sea ice, high productivity, and dicothermal
455 species (Fig. 7), indicating seasonal sea ice with highly stratified waters during the ice-
456 melt season. Nitrogen isotopes indicate high nutrient utilization (Fig. 7) consistent with
457 nitrogen-limited productivity in stratified waters as well as localized denitrification.
458 Numerous shell fragments, two sand layers and the highest percentages of clay-sized
459 sediments in the record were deposited during MIS 12 (Figs 4 and 8) indicating input of
460 terrigenous material, however, crossplots of elemental (C_{org}/N or N/C_{org}) and isotopic

461 ($\delta^{13}\text{C}$, $\delta^{15}\text{N}$) indicators of terrigenous and marine carbon pools indicate that the organic
462 matter during MIS 12 is a diverse mix of marine phytoplankton and soil detritus (Fig. 8)
463 likely derived from in-situ, but low, productivity and transport by several methods
464 including large, oligotrophic rivers and downslope transport. Glacial ice was likely
465 restricted to mountain-valley glaciers, similar to the last glacial maximum (e.g.
466 Glushkova, 2001). These small, distant glaciers would not have produced large amounts
467 of ice bergs though occasional glacial ice rafted debris (IRD) may have come from the
468 Koryak Mountains, the Aleutians or Beringia. Consistent with this, sediments typical of
469 glacial IRD, such as dropstones, are sparse, but present. In addition, sea ice rafting tends
470 to preferentially entrain clay and silt (Reimnitz et al., 1998) and is likely to be an
471 important contributor of terrigenous sediments.

472

473 **5.1.2 Termination V (425-423 ka)**

474 Termination V is the transition from MIS 12 to MIS 11. Worldwide, it is a rapid
475 deglaciation that is followed by a long (up to 30 kyrs) climate optimum (Milker et al.,
476 2013). At U1345, gradually increasing productivity coupled with decreasing nutrient
477 utilization and sea ice occurs between 425 and 423 ka. This is seen as an increase in
478 absolute diatom abundances and relative percent abundance of *Chaetoceros* RS and a
479 decrease in sea ice diatoms and $\delta^{15}\text{N}$ values (Fig. 7). It is plausible that increased nitrogen
480 availability drove higher primary productivity as floods scoured fresh organic matter
481 from the submerging continental shelf (Bertrand et al., 2000). Rapid input of bioavailable
482 nitrogen as the shelf was inundated has been suggested to explain increasing productivity
483 during the last deglaciation in the Sea of Okhotsk (Shiga and Koizumi, 2000) and during
484 MIS 11 in the North Atlantic (Poli et al., 2010) and also may have contributed to dysoxia
485 by ramping up nutrient recycling, bacterial respiration, and decomposition of organic
486 matter in the Bering Sea.

487

488 **5.1.3 Peak MIS 11 (423-394 ka)**

489 Globally, peak interglacial conditions (often referred to as MIS 11.3 or 11c) are centered
490 around 400 to 410 ka (Dutton et al., 2015; Raymo and Mitrovica, 2012), though the exact
491 interval of the temperature optimum varies globally and lasted anywhere from 10 to 30
492 kyrs (Kandiano et al., 2012; Kariya et al., 2010; Milker et al., 2013). At U1345, peak
493 interglacial conditions begin during the Termination V Laminations at 423 ka and
494 continue until 394 ka, lasting nearly 30 kyrs consistent with the synthesis of the PAGES
495 Past Interglacials working group (2016).

496

497 **5.1.3.1 Laminations (423-410 ka)**

498 A 3.5 m thick laminated interval is deposited during early MIS 11 beginning at 423 ka
499 (Fig. 7) when insolation was high at 65°N (Berger and Loutre, 1991). Its presence
500 indicates that the bottom water at 1,000 m in the Bering Sea was dysoxic for more than
501 11 kyrs. These laminations are characterized as Type I laminations with a high diatom
502 content (Fig. 4). Several lines of evidence point towards high productivity among
503 multiple phytoplankton groups as opposed to simply a change in preservation. First, we
504 see an increase in diatom abundances by two orders of magnitude increase since MIS 12,
505 second, a low-diversity diatom assemblage dominated by *Chaetoceros* RS, third, an
506 abrupt increase in percent organic carbon, and fourth, high percent CaCO₃ and abundant
507 calcareous nannofossils dominated by small *Gephyrocapsa*. Furthermore, enriched $\delta^{15}\text{N}$
508 values indicate either increased nitrogen utilization that likely led to this increased
509 productivity or localized denitrification in low oxygen waters (Fig. 7).

510 Sea ice extent decreases during this interval with no eponitic diatoms present and reduced
511 amounts of sea ice diatoms found in both eponitic and marginal ice (Fig. 7). Geochemical
512 crossplots indicate a high contribution from soil detritus and C3 plant organic matter (Fig.
513 8). At the onset of the laminated interval (423 ka), $\delta^{13}\text{C}$ decreases and $\text{C}_{\text{org}}/\text{N}$ increases
514 rapidly (Fig. 7) as the tundra-covered Bering Sea shelf is flooded.

515 However, the diatom record during the laminated interval has the lowest contribution of
516 neritic diatoms and virtually no fresh water diatoms (Fig. 7), suggesting that although

Beth Caissie 8/11/2016 12:30 AM

Deleted: is reduced

Beth Caissie 8/11/2016 12:30 AM

Deleted: almost

Beth Caissie 8/11/2016 12:31 AM

Deleted: other

520 terrigenous organic matter was an important input at the site, coastal, river, or
521 swamp/tundra diatoms were not carried out to U1345 with this terrigenous organic
522 matter.

523

524 **5.1.3.2 Post Laminations (410-394 ka)**

525 Both high N/C_{org} and $\delta^{13}C$ indicate that input of terrigenous organic matter is highest at
526 the onset of the Termination V Laminations and then declines until mid MIS 11 (400 ka)
527 at which time the organic matter is largely derived from marine phytoplankton (Fig. 7;
528 red to grey dots in Fig. 8). This may be related to rising eustatic sea level causing the
529 migration of the paleoshoreline farther northward and away from U1345.

530 Throughout MIS 11, *Chaetoceros* RS, a species indicative of high productivity, is
531 generally higher when insolation is higher and lower when insolation is lower (404-390
532 ka; Fig. 7). However, although their fluctuations are small, warm water species show the
533 opposite trend, with higher proportions of warm water diatoms when insolation is low
534 (Fig. 7). If higher proportions of warm water diatoms indicate warmer water, then this
535 suggests that productivity is highest in colder waters but when insolation is high, and
536 lowest in warmer waters when insolation is low. This may reveal a relationship between
537 upwelling of colder waters and high productivity.

538

539 **5.1.4 Late MIS 11 to MIS 10 (younger than 394 ka)**

540 After 394 ka, diatom productivity indicators are the lowest in the record but linearly
541 increase to the top of the record. This is in contrast to a slight increase in diatom
542 abundance, which increases at 393 ka and then remains relatively stable into MIS 10. Sea
543 ice indicators also remain relatively high from 392 to the top of the record and
544 dicothermal species reflect moderately stratified waters. Warm water species decrease
545 from 390 ka to the top of the record (Fig. 7). The sum of this evidence indicates that at
546 the end of MIS 11, summers were warm and sea ice occurred seasonally, perhaps lasting
547 a bit longer than at other times in the record.

548 Eustatic sea level decreased beginning about 402 ka (Rohling et al., 2010), but sea level
549 remained high enough to allow *N. seminae* to reach the shelf slope break until about 380
550 ka (Fig. 7).

551

552 **5.2 The Bering Sea in the Context of Regional and Global Variability**

553 Across the Bering Sea, sediments at sites near Bowers Ridge (Fig. 1) are dominated by
554 opal during MIS 11 (Kanematsu et al., 2013); whereas, biogenic sediments at sites along
555 the Bering Slope, including U1345, are diluted by sea ice transport of lithogenic
556 sediments as well as down-slope sediment transport (Kanematsu et al., 2013). However,
557 the rate of biogenic opal accumulation is comparable for all sites in the Bering Sea,
558 despite differences in sedimentation rates (Kanematsu et al., 2013; Stroynowski et al.,
559 2015). Opal content in the sediments varies on glacial/interglacial time scales with high
560 productivity during interglacials. Indeed, the highest percent opal concentration of the
561 past 1 Ma occurs during MIS 11 at the two slope sites, U1345 and U1343 (Kanematsu et
562 al., 2013).

563 Biogenic opal increases during early MIS 11 at Sites U1343 and U1345 (Kanematsu et
564 al., 2013). At U1345, it mimics the pattern of relative percent abundance of *Chaetoceros*
565 RS, the most abundant productivity indicator (Fig. 9). Although diatom data from other
566 cored sites is low resolution (1-4 samples during MIS 11) (Kato et al., 2016; Onodera et
567 al., 2016; Stroynowski et al., 2015; Teraishi et al., 2016), it provides a snapshot of diatom
568 assemblages during MIS 11. Sea ice diatoms contribute approximately 30% of the diatom
569 assemblages at the two slope sites, U1345 (this study) and U1343 (Teraishi et al., 2016),
570 between 10 and 20% of the assemblage at the eastern Bowers Ridge site (U1340)
571 (Stroynowski et al., 2015), but less than 2% of the assemblage on the western flanks of
572 Bowers Ridge (U1341) (Onodera et al., 2016). In the North Pacific (ODP Site 884), no
573 sea ice diatoms are present during MIS 11 (Kato et al., 2016). Site U1341 contained an
574 assemblage high in dicothermal indicators such as *Shionodiscus trifultus*, and
575 *Actinocyclus curvatulus*, oceanic front indicators such as *Rhizosolenia hebetata*, and *N.*
576 *seminae* (Onodera et al., 2016), while the North Pacific (Site 884) assemblage is
577 dominated by dicothermal indicators during MIS 11 (Kato et al., 2016). Percent opal

578 declines at Bowers Ridge during early MIS 11 at the same time as it increases at the slope
579 sites (Iwasaki et al., 2016) (Fig. 9) when sea ice is reduced and upwelling along the shelf-
580 slope break is increased. This implies that the relationship between productivity and sea
581 ice in the Bering Sea is perhaps more complex than the simple idea that sea ice inhibits
582 productivity (Iwasaki et al., 2016; Kim et al., 2016). The region is strongly influenced by
583 winter sea ice throughout MIS 11 with seasonal sea ice present farther south along the
584 slope than today and also in the eastern Bering Sea. Highly stratified waters, perhaps due
585 to the seasonal expansion and retreat of sea ice, extended across the entire basin and even
586 into the North Pacific.

587 Local ventilation of North Pacific Intermediate Water decreased as Bering Strait opened
588 during Termination V with the weakest ventilation occurring around 400 ka (Knudson
589 and Ravelo, 2015). This is coeval with the highest relative percent abundances of
590 dicothermal diatoms indicating highly stratified water (Fig. 9).

591

592 **5.2.1 Temperature and Aridity during MIS 11**

593 When sea level was low during glacial periods such as MIS 12 (Rohling et al., 2010),
594 U1345 was proximal to the Beringian coast (Fig. 2). With the Bering land bridge
595 exposed, the continent was relatively cold and arid (Glushkova, 2001). In western
596 Beringia, Lake El'gygytgyn was perennially covered with ice, summer air temperatures
597 were warming in sync with increasing insolation from 4 to 12° C, but annual precipitation
598 was low (200-400 mm) (Vogel et al., 2013).

599 As sea level rose, and global ice volume reached the lowest amount for the past 500 kyrs
600 (Lisiecki and Raymo, 2005), the generally continental temperatures in the Northern
601 Hemisphere increased (D'Anjou et al., 2013; de Vernal and Hillaire-Marcel, 2008;
602 Lozhkin and Anderson, 2013; Lyle et al., 2001; Melles et al., 2012; Pol, 2011;
603 Prokopenko et al., 2010; Raynaud et al., 2005; Tarasov et al., 2011; Tzedakis, 2010;
604 Vogel et al., 2013) with a northward expansion of boreal forests in Beringia (Kleinen et
605 al., 2014). However, the marine realm does not reflect this warming as strongly. At
606 U1345, the relative percent warm water species suggest that SSTs during peak MIS 11
607 were only slightly warmer than during MIS 12. Indeed, MIS 11 is not the warmest

608 interglacial in most marine records (Candy et al., 2014), rather MIS 5e is the warmest
609 many places (PAGES et al., 2016). This is especially evident in the Nordic Seas where
610 MIS 11 SSTs were lower than Holocene values (Bauch et al., 2000). However, MIS 11 is
611 unique because it was much longer than MIS 5e in all records (PAGES et al., 2016). One
612 exception to this is the Arctic Ocean, which was warm enough during MIS 11 to imply
613 increased Pacific water input through Bering Strait (Cronin et al., 2013).

614 With elevated sea level, peak MIS 11c was very humid in many places. In the Bering
615 Sea, modeling studies estimate up to 50 mm more precipitation than today at 410 ka
616 (Kleinen et al., 2014). The most humid, least continental period recorded in the sediments
617 at Lake Baikal occurs from 420-405 ka (Prokopenko et al., 2010), and extremely high
618 precipitation is recorded at Lake El'gygytyn on the nearby Chukotka Peninsula from
619 420-400 ka (Melles et al., 2012).

620

621 **5.2.2 Millennial-Scale Laminations and Changes in Sea Ice**

622 Globally, late MIS 11 is characterized as a series of warm and cold cycles (Candy et al.,
623 2014; Voelker et al., 2010), though there is no agreement on the timing of these cycles.
624 At Site U1345, laminations are deposited intermittently between 394 and 392 ka and
625 again after 375 ka (Fig. 4) as the climate transitioned into MIS 10. These laminations are
626 quite different from the Termination V Laminations due to their shorter duration and lack
627 of obvious shift in terrigenous vs. marine carbon source. In addition, these Type II
628 laminations have higher diatom abundances and CaCO₃, but lack increased upwelling
629 indicators. Primary production during these laminations is likely not driven by nutrient
630 upwelling along the shelf-slope break. Instead, most of these laminations show an
631 increase in sea ice diatoms and roughly correspond with millennial scale stadial events
632 that occurred during late MIS 11 in the North Atlantic (Fig. 9) (Voelker et al., 2010) as
633 well as carbonate peaks at Blake Ridge (Chaisson et al., 2002). This suggests
634 teleconnections between the Bering Sea and the North Atlantic at this time and places an
635 indirect constraint on the depth of the Bering Strait sill.

636 | It is possible to note that the laminations occur at a time when global sea level was
637 fluctuating near the sill depth of Bering Strait (-50 m amsl) (Rohling et al., 2010) (see

Beth Caissie 8/4/2016 1:20 PM

Deleted: tantalizing

639 grey line at -50 m on Fig. 9). When sea level fluctuates near this level, Bering Strait
640 modulates widespread climate changes that see-saw between the Atlantic and Pacific
641 regions on millennial-scale time frames (Hu et al., 2010). And when Bering Strait is
642 closed, North Pacific Intermediate Water formation increases (Knudson and Ravelo,
643 2015). Further study will elucidate these connections.

644 A “Younger Dryas-like” temperature reversal is seen midway through Termination V in
645 the North Atlantic (Voelker et al., 2010), Antarctica (EPICA Community Members,
646 2004) and at Lake El’gygytgyn (Vogel et al., 2013), however there is no evidence for
647 such an event in the Bering Sea.

648

649 **5.2.3 Anomalous Interval (405-394 ka)**

650 The interval between 405 and 394 ka contains a number of unusual characteristics.
651 Diatom assemblages are similar to those found in nearshore sediments from the Anvillian
652 Transgression 800 km northeast of U1345 in Kotzebue Sound (Fig. 1) (Pushkar et al.,
653 1999). A large peak in neritic species occurs at 404 ka followed by the highest relative
654 percentages of fresh water species at the site and a slight increase in sea ice diatoms from
655 400 to 394 ka (Fig. 7, grey bar). Primary productivity was low during this interval with
656 the highest $\delta^{15}\text{N}$ values of MIS 11, likely indicating denitrification. However, two large
657 depletions in $\delta^{15}\text{N}$ bracket this interval and occur as *Chaetoceros* RS decrease in relative
658 percent abundance (Fig. 10). The organic matter is primarily sourced from marine
659 phytoplankton, similar to the organic matter found during the two glacial intervals and
660 distinctly different from the organic matter found during the rest of peak MIS 11 (Fig. 8).
661 Detailed grain size analysis shows a fining upward trend of clay sized grains as well as a
662 broad increase in sand sized grains and in particular grains greater than 250 μm (Fig. 10).
663 All samples are poorly to very poorly sorted (See Supplemental Material). Shipboard data
664 shows an increase in the presence of pebbles, several sand layers (Fig. 10), and a thick
665 interval of silty sand (Takahashi et al., 2011) at 404 ka (Fig. 4). While the presence of
666 coarse material implies a terrestrial source for the sediments during this interval, this
667 terrestrial matter must have been largely devoid of organic matter. The sum of this
668 evidence leads us to investigate further three different interpretations of the interval

669 highlighted in grey on Fig. 10: a reversal of flow through Bering Strait, a tidewater
670 glacial advance, and a turbidite.

671

672 **5.2.3.1 Reversal of Bering Strait Through Flow**

673 As sea level rose after MIS 12, the connection between the Pacific and the Atlantic was
674 reestablished via Bering Strait. De Boer and Nof (2004) suggest that under high sea level
675 conditions, if freshwater is suddenly released into the North Atlantic, the Bering Strait
676 might act as an “exhaust valve” allowing fresh water from the Arctic Basin and the North
677 Atlantic to flow into the Arctic Ocean and then flow south through the Bering Strait, thus
678 preventing a shut-down in thermohaline circulation (DeBoer and Nof, 2004).

679 On St. Lawrence Island (Fig. 1), evidence for Arctic mollusks entering the Gulf of
680 Anadyr suggests that flow through Bering Strait was reversed at some point during the
681 Middle Pleistocene (Hopkins, 1972). Unfortunately, this event is poorly dated.

682 If flow were reversed due to a meltwater event (DeBoer and Nof, 2004), we would expect
683 a temporary reduction in North Atlantic Deep Water (NADW) formation and an increase
684 in southerly winds from Antarctica (DeBoer and Nof, 2004). In the Bering Sea, we would
685 expect to see an increase in common Arctic or Bering Strait diatom species and a
686 decrease in North Pacific indicators. In addition, the clay minerals in the Arctic Ocean are
687 overwhelmingly dominated by illite (Ortiz et al., 2012), which tends to adsorb large
688 amounts of ammonium (Schubert and Calvert, 2001). So, if net flow were to the south,
689 one might expect to find increased illite and decreased C_{org}/N and $\delta^{15}N$ values.

690 Proxy evidence for NADW ventilation indicates that between 412 and 392 ka, NADW
691 formation decreased for short periods (< 1 ka) (Poli et al., 2010). In contrast, AABW
692 formation appears to have drastically slowed around 404 ka, suggesting a decrease in sea
693 ice and winds from around Antarctica as the southern hemisphere warmed (Hall et al.,
694 2001).

695 At U1345, diversity is highest around 400 ka, due to the multiple contributions of Arctic
696 species (fresh water, shelf, coastal, sea ice) and common pelagic diatoms, while the North
697 Pacific indicator, *N. seminae* maintains low relative abundances and does not change
698 throughout this interval. No marked increase in illite is observed during this interval in

699 either U1345 or elsewhere on the Bering Slope (Kim et al., 2016) (Fig. 9). However,
700 chlorite, which dominates North Pacific sediments (Ortiz et al., 2012) decreases at 399 ka
701 (Fig. 9), suggesting a reduced Pacific influence. C_{org}/N values began decreasing linearly
702 starting at 409 ka, productivity sharply decreases at 406 ka, $\delta^{15}N$ values are the most
703 depleted at 405 ka, just 1 kyr before a conspicuous peak in *P. sulcata*, a common diatom
704 found in the Bering Strait. Because there is conflicting evidence of both northward and
705 southward flow, we reject the hypothesis of reversed flow through Bering Strait during
706 MIS 11.

707

708 **5.2.3.2 Glacial Advance**

709 At its maximum, the Nome River Glaciation is the most extensive glaciation in central
710 Beringia and is dated to Middle Pleistocene. Although it has not been precisely dated, it
711 is likely correlative with late MIS 11 or MIS 10 (Kaufman et al., 1991; Miller et al.,
712 2009). Nome River glaciomarine sediments recording the onset of rapid tidewater glacial
713 advance are found in places such as St. Lawrence Island (Gualtieri and Brigham-Grette,
714 2001; Hopkins, 1972), the Pribilof Islands (Hopkins, 1966), the Alaska Arctic coastal
715 plain (Kaufman and Brigham-Grette, 1993), Kotzebue (Huston et al., 1990), Nome
716 (Kaufman, 1992), and Bristol Bay (Kaufman et al., 2001) (Fig. 1). At these sites glaciers
717 advanced, in some cases more than 200 km, and reached tidewater while eustatic sea
718 level was high (Huston et al., 1990).

719 Although global sea level was near its maximum, and much of the world was
720 experiencing peak MIS 11 conditions (Candy et al., 2014), there is evidence that the high
721 latitudes were already cooling. At 410 ka, insolation at 65° N began to decline (Berger
722 and Loutre, 1991), and cooling began at 407 ka in Antarctica, expressed both isotopically
723 and as an expansion of sea ice (Pol, 2011). Millennial scale cooling events were recorded
724 at Lake Baikal (Prokopenko et al., 2010). By 405 ka, there was some evidence globally
725 for ice sheet growth (Milker et al., 2013) as Lake Baikal began to shift towards a dryer,
726 more continental climate (Prokopenko et al., 2010) and productivity declined at Lake
727 El'gygytgyn (Melles et al., 2012).

Beth Caissie 8/11/2016 12:20 AM
Deleted: 407

729 Solar forcing coupled with a proximal moisture source, the flooded Beringian shelf,
730 drove snow buildup (Brigham-Grette et al., 2001; Huston et al., 1990; Pushkar et al.,
731 1999) and glacial advance from coastal mountain systems. Precipitation at Lake
732 El'gygytgyn, just west of the Bering Strait, was two to three times higher than today at
733 405 ka (Melles et al., 2012). A similar "snow gun" hypothesis has been invoked for other
734 high latitude glaciations (Miller and De Vernal, 1992); however, Beringia is uniquely
735 situated. Once sea level began to drop, Beringia became more continental and arid
736 (Prokopenko et al., 2010) and the moisture source for these glaciers was quickly cut off.

737 Subaerial and glaciofluvial deposits below the Nome River tills and correlative
738 glaciations indicate that Beringian ice, especially from the western Brooks Range,
739 advanced as the climate grew colder. Ice wedges and evidence of permafrost are common
740 (Huston et al., 1990; Pushkar et al., 1999) in sand and gravel deposits later overridden by
741 Nome River till.

742 If evidence of the Nome River glaciation in central Beringia was present at U1345, we
743 might expect to see evidence of glacial ice rafting. Previous work has suggested that
744 sediments deposited by icebergs should be poorly sorted and skew towards coarser
745 sediments (Nürnberg et al., 1994). Sediments greater than 150 μm are likely glacially ice
746 rafted (St. John, 2008), however it is not possible to distinguish sediments deposited by
747 glacial versus sea ice on grain size alone (St. John, 2008). Both types of ice commonly
748 carry sand-sized or larger sediments (Nürnberg et al., 1994). Sea ice diatoms should not
749 be found in glacial ice, instead, we would expect glacial ice to be either barren, or to
750 carry fresh water diatoms from ice-scoured lake and pond sediments. At U1345, there is a
751 brief coarse interval (405-402 ka) followed by deposition of fresh water diatoms until 394
752 ka.

753 Although it is tempting to assign this to the Nome River Glaciation, there are too many
754 unknowns including whether the coarse grains were transported by sea ice, glacial ice, or
755 some other method. Further work is ongoing to look for the onset of the Nome River
756 Glaciation in both MIS 11 and MIS 13 as well as to distinguish the transport mechanism
757 for these quartz grains.

758

759 **5.2.3.3 Turbidite**

760 The location of Site U1345 on a high interfluvium was chosen to minimize the likelihood
761 that sediments could have been transported and deposited here by turbidites or other
762 down-slope currents, yet evidence for a turbidite during this interval is very strong.
763 Although there is no evidence of slumping or distorted sediments, clear erosive surfaces,
764 or any structures that would indicate a turbidite during the anomalous interval, there are
765 folded laminations elsewhere in the sediment core (Takahashi et al., 2011). If this interval
766 was a turbidite, we would expect an erosive surface, overlain by clasts and perhaps a
767 coarse sand layer followed by a fining up sequence. We see intermittent sand layers and
768 small pebbles coupled with a linear increase in the percent clay throughout the interval
769 (Fig. 10). Sediments are poorly sorted throughout the interval, consistent with rapid
770 turbidite deposition and the presence of neritic and fresh water diatoms suggest
771 redeposition of these sediments offshore from shallow water. Sancetta and Robinson
772 (1983) argue that benthic pennate species were transported out of shallow water by rivers
773 and turbidity currents during glacial periods; however, they do not consider ice as a
774 transport mechanism. In this study, we have considered most benthic pennate species as
775 members of either the eponitic or both ice ecological niches (von Quillfeldt et al., 2003).
776 However, it is striking that the pattern of benthic pennate species at U1345 is nearly
777 identical to that of the fresh water species.

778 Although the evidence is strongest for a turbidite, it is unusual to find just one turbidite as
779 we might expect a turbidity flow to exist in the same place for a prolonged period.
780 Further investigation of this and other Bering Sea cores can elucidate how common
781 intervals like this are along the slope and if there is temporal consistency between
782 deposits. The presence of a turbidite may suggest that the age model for this core needs to
783 be slightly revised; however, there is no evidence of an erosive surface, nor a clear
784 indication that all of the material deposited during this interval is allochthonous. In
785 addition, the presence of a turbidite does not change the overall orbital and millennial
786 scale interpretations of this record. Therefore, we choose to keep the age model as is.

787

788 **6 Conclusions**

789 This study aimed to describe orbital- and millennial-scale changes in productivity and sea
790 ice extent in the Bering Sea, specifically at the shelf-slope break Site U1345. We further
791 tested two hypotheses: 1) in Beringia, tidewater glaciers advanced while sea level was
792 high and 2) Bering Strait Through Flow reversed shortly after the MIS 12 glacial
793 termination (Termination V).

794 The interval between MIS 12 and MIS 10 is marked by large changes in productivity but
795 only minor changes in sea ice extent at Site U1345. Productivity changed in concert with
796 changes in insolation and water temperature. During warmer periods, high stratification
797 appears to have led to lowered productivity. Site U1345 sites in the present-day oxygen
798 minimum zone, and the presence of laminations frequently throughout the core indicates
799 that oxygen is low. Evidence of denitrification is prevalent for much of the record, likely
800 due to dysoxic conditions.

801 During MIS 12, productivity was low and seasonal sea ice dominated the Bering Sea with
802 highly stratified waters during the ice-melt season. At Termination V, diatom
803 productivity increased by two orders of magnitude while nitrogen utilization decreased.
804 At 423 ka, an 11 kyr long laminated interval began. This interval was highly productive
805 for multiple phytoplankton groups. The surface waters were relatively unstratified, and
806 sea ice, though still present, decreased. This period is marked by the highest terrigenous
807 organic matter input of the record possibly due to scouring of the continental shelf as sea
808 level rose. During peak and late MIS 11, SSTs appear to have been warm, but seasonal
809 sea ice lasted longer. And at the end of MIS 11, sea ice increased as sea level declined.

810 Laminations at the end of MIS 11 correspond with millennial scale stadials seen in the N
811 Atlantic. These deposits represent possible evidence of teleconnections between the
812 Atlantic and the Pacific as eustatic sea level fluctuated near the Bering Strait sill depth.

813 Decreased NADW formation and species transport from the Arctic Ocean southward
814 support a reversal of the Bering Strait Current at 405 ka; however, there is no evidence
815 for the transport of Arctic Ocean clay minerals or oceanographic forcing related to an
816 increase in winds in Antarctica. Therefore, there is inconclusive evidence for a reversal of
817 the Bering Strait Current during MIS 11.

818 When global sea level was at its maximum, insolation dropped and Beringia began to
819 cool in sync with other polar regions. Sediments deposited during the so called,
820 “anomalous interval” may have been carried by tidewater glaciers bringing neritic species
821 far off shore. This glacial advance is attributed to humid conditions in Beringia that
822 allowed rapid glacial growth. Alternatively, this interval may be a turbidite which could
823 shift the age model for this core and cause this section to be omitted from the
824 paleoceanographic record.

825 Previous studies have referred to MIS 11 as an analog for the next century of climate
826 change. Today sea ice barely reaches Site U1345 even in winter and does not reach any
827 other Bering Sea or North Pacific sites (U1340, U1341, U1343 or ODP 884). In contrast,
828 during MIS 11, sea ice diatoms are present throughout the entirety of MIS 11 at U1345
829 and seasonal sea ice appears to have reached both slope sites and the eastern Bowers
830 Ridge (Onodera et al., 2016; Stroynowski et al., 2015; Teraishi et al., 2016). However,
831 evidence for a reduction of sea ice in the Arctic Ocean during MIS 11 (Cronin et al.,
832 2013) implies that while winter sea ice was expanded in the Bering Sea compared to
833 today, summer sea ice was likely reduced. Such a significant difference may indicate that
834 MIS 11 is not an ideal analog for climate change over the next 100 years.

835 However, there are lessons to be learned from the paleo-record. When sea ice declined
836 during early MIS 11, nutrients were upwelled from the deep Bering Sea and flooding of
837 the land bridge further brought nutrients into the surface waters. This caused productivity
838 to increase at Sites U1345 and U1343. However, at Bowers Ridge Site U1341,
839 productivity declined at this time. The pattern of primary productivity across the Bering
840 Sea underscores that understanding the myriad drivers of primary productivity is essential
841 as we prepared for decreased sea ice in the future.

842 Data used in this manuscript are archived at the National Center for Environmental
843 Information (<https://www.ncdc.noaa.gov/paleo/study/20326>),

844

845 Acknowledgements

846 The authors thank the captain and crew of the JOIDES Resolution and Exp. 323 co-chief
847 scientists Christina Ravelo and Kozo Takahashi. We acknowledge the two reviewers,

Beth Caissie 8/11/2016 12:38 AM

Formatted: Normal, Left, Space Before: 0 pt, Line spacing: single

Beth Caissie 8/11/2016 12:38 AM

Deleted: <https://www.ncei.noaa.gov>; specific doi and web address pending

Beth Caissie 8/11/2016 12:38 AM

Formatted: Font:Times, 10 pt

850 Thomas Cronin and Jason Addison who provided us with thoughtful comments that
851 greatly improved this manuscript. This work was partially supported by National Science
852 Foundation, Office of Polar Programs Arctic Natural Sciences Award #1023537 and a
853 | Post Expedition Award from the Consortium for Ocean Leadership.

854 **References**

- 855 Aizawa, C., Tanimoto, M., and Jordan, R. W.: Living diatom assemblages from North
856 Pacific and Bering Sea surface waters during summer 1999, *Deep-Sea Research Part II-*
857 *Topical Studies in Oceanography*, 52, 2186-2205, 2005.
- 858 Alexander, V. and Chapman, T.: The role of epontic algal communities in Bering Sea ice.
859 In: *The Eastern Bering Sea Shelf: Oceanography and Resources*, Hood, D. W. and
860 Calder, J. A. (Eds.), University of Washington Press, Seattle, Washington, 1981.
- 861 Asahi, H., Kender, S., Ikehara, M., Sakamoto, T., Takahashi, K., Ravelo, A. C., Alvarez
862 Zarikian, C. A., Khim, B. K., and Leng, M. J.: Orbital-scale benthic foraminiferal oxygen
863 isotope stratigraphy at the northern Bering Sea Slope Site U1343 (IODP Expedition 323)
864 and its Pleistocene paleoceanographic significance, *Deep Sea Research Part II: Topical*
865 *Studies in Oceanography*, 125–126, 66-83, 2016.
- 866 Barr, I. D. and Clark, C. D.: Distribution and pattern of moraines in Far NE Russia reveal
867 former glacial extent, *Journal of Maps*, 5, 186-193, 2009.
- 868 Barron, J. A., Bukry, D., Dean, W. E., Addison, J. A., and Finney, B.: Paleooceanography
869 of the Gulf of Alaska during the past 15,000 years: results from diatoms, silicoflagellates,
870 and geochemistry, *Marine Micropaleontology*, 72, 176-195, 2009.
- 871 Bauch, H. A., Erlenkeuse, H., Helmke, J. P., and Struck, U.: A paleoclimatic evaluation
872 of marine oxygen isotope stage 11 in the high-northern Atlantic (Nordic seas), *Global and*
873 *Planetary Change*, 24, 27-39, 2000.
- 874 Berger, A., Crucifix, M., Hodell, D. A., Mangili, C., McManus, J. F., Otto-Bliesner, B.,
875 Pol, K., Raynaud, D., Skinner, L. C., Tzedakis, P. C., Wolff, E. W., Yin, Q. Z., Abe-
876 Ouchi, A., Barbante, C., Brovkin, V., Cacho, I., Capron, E., Ferretti, P., Ganopolski, A.,
877 Grimalt, J. O., Hönisch, B., Kawamura, K., Landais, A., Margari, V., Martrat, B.,
878 Masson-Delmotte, V., Mokeddem, Z., Parrenin, F., Prokopenko, A. A., Rashid, H.,

879 Schulz, M., and Vazquez Riveiros, N.: "Interglacials of the last 800,000 years", Rev
880 Geophys, doi: 10.1002/2015RG000482, 2015. n/a-n/a, 2015.

881 Berger, A. and Loutre, M. F.: Insolation Values for the Climate of the Last 10 Million
882 Years, *Quaternary Science Reviews*, 10, 297-317, 1991.

883 Bertrand, P., Pedersen, T. F., Martinez, P., Calvert, S., and Shimmield, G.: Sea level
884 impact on nutrient cycling in coastal upwelling areas during deglaciation: evidence from
885 nitrogen isotopes, *Global Biogeochemical Cycles*, 14, 341-355, 2000.

886 Bowen, D. Q.: Sea level ~400 000 years ago (MIS 11): analogue for present and future
887 sea-level?, *Clim Past*, 6, 19-29, 2010.

888 Brigham-Grette, J., Hopkins, D. M., Ivanov, V. F., Basilyan, A. E., Benson, S. L., Heiser,
889 P. A., and Pushkar, V. S.: Last interglacial (isotope stage 5) glacial and sea-level history
890 of coastal Chukotka Peninsula and St. Lawrence Island, Western Beringia, *Quaternary
891 Science Reviews*, 20, 419-436, 2001.

892 Brunelle, B. G., Sigman, D. M., Cook, M. S., Keigwin, L., Haug, G. H., Plessen, B.,
893 Schettler, G., and Jaccard, S. L.: Evidence from diatom-bound nitrogen isotopes for
894 subarctic Pacific stratification during the last ice age and a link to North Pacific
895 denitrification changes, *Paleoceanography*, 22, 2007.

896 Caissie, B. E.: Diatoms as recorders of sea ice in the Bering and Chukchi seas: proxy
897 development and application, PhD, Geosciences, University of Massachusetts Amherst,
898 Amherst, MA, 190 pp., 2012.

899 Caissie, B. E., Brigham-Grette, J., Lawrence, K. T., Herbert, T. D., and Cook, M. S.: Last
900 Glacial Maximum to Holocene sea surface conditions at Umnak Plateau, Bering Sea, as
901 inferred from diatom, alkenone, and stable isotope records, *Paleoceanography*, 25,
902 10.1029/2008pa001671, 2010.

903 Candy, I., Schreve, D. C., Sherriff, J., and Tye, G. J.: Marine Isotope Stage 11:
904 Palaeoclimates, palaeoenvironments and its role as an analogue for the current
905 interglacial, *Earth-Science Reviews*, 128, 18-51, 2014.

906 Cavalieri, D. J., Parkinson, P., Gloersen, P., and Zwally: Sea Ice Concentrations from
907 Nimbus-7 SMMR and DMSP SSM/I Passive Microwave Data, 1996-2008. National
908 Snow and Ice Data Center, Boulder, CO, 1996.

909 Chaisson, W. P., Poli, M. S., and Thunell, R. C.: Gulf Stream and Western Boundary
910 Undercurrent variations during MIS 10 -12 at Site 1056, Blake-Bahama Outer Ridge,
911 *Marine Geology*, 189, 79-105, 2002.

912 Cook, M. S., Ravelo, A. C., Mix, A., Nesbitt, I. M., and Miller, N. V.: Tracing subarctic
913 Pacific water masses with benthic foraminiferal stable isotopes during the LGM and late
914 Pleistocene, *Deep Sea Research Part II: Topical Studies in Oceanography*, 125–126, 84-
915 95, 2016.

916 Cooper, L. W., Whitedge, T. E., Grebmeier, J. M., and Wieingartner, T.: The nutrient,
917 salinity, and stable oxygen isotope composition of Bering and Chukchi Seas waters in
918 and near the Bering Strait, *Journal of Geophysical Research*, 102, 12563-12573, 1997.

919 Cronin, T. M., Polyak, L., Reed, D., Kandiano, E. S., Marzen, R. E., and Council, E. A.:
920 A 600-ka Arctic sea-ice record from Mendeleev Ridge based on ostracodes, *Quaternary
921 Science Reviews*, 79, 157-167, 2013.

922 D'Anjou, R. M., Wei, J. H., Casteneda, I. S., Brigham-Grette, J., Petsch, S. T., and
923 Finkelstein, D. B.: High-latitude environmental change during MIS 9 and 11:
924 biogeochemical evidence from Lake El'gygytgyn, Far East Russia, *Clim Past*, 9, 567-581,
925 2013.

926 de Vernal, A. and Hillaire-Marcel, C.: Natural variability of Greenland climate,
927 vegetation, and ice volume during the past million years, *Science*, 320, 1622-1625, 2008.

928 DeBoer, A. M. and Nof, D.: The Exhaust Valve of the North Atlantic, *Journal of Climate*,
929 17, 417-422, 2004.

930 Dickson, A. J., Beer, C. J., Dempsey, C., Maslin, M. A., Bendle, J. A., McClymont, E. L.,
931 and Pancost, R. D.: Oceanic forcing of the Marine Isotope Stage 11 interglacial, *Nature*
932 *Geoscience*, 2, 428-433, 2009.

933 Droxler, A. W., Alley, R. B., Howard, W. R., Poore, R. Z., and Burckle, L. H.: Unique
934 and exceptionally long interglacial Marine Isotope Stage 11: window into Earth's warm
935 future climate. In: *Earth's Climate and Orbital Eccentricity: The Marine Isotope Stage 11*
936 *Question*, Droxler, A. W., Poore, R. Z., and Burckle, L. H. (Eds.), American Geophysical
937 Union, Washington, DC, 2003.

938 Dutton, A., Carlson, A. E., Long, A. J., Milne, G. A., Clark, P. U., DeConto, R., Horton,
939 B. P., Rahmstorf, S., and Raymo, M. E.: Sea-level rise due to polar ice-sheet mass loss
940 during past warm periods, *Science*, 349, 2015.

941 Eberl, D. D.: User's Guide to RockJock--a Program for Determining Quantitative
942 Mineralogy from Powder X-Ray Diffraction Data, US Geological Survey, Open-File
943 Report 03-78, Boulder, CO, 2003.

944 EPICA Community Members: Eight glacial cycles from an Antarctic ice core, *Nature*,
945 429, 623-628, 2004.

946 Flores, J. A., Gersonde, R., and Sierro, F. J.: Pleistocene fluctuations in the Agulhas
947 Current Retroflexion based on the calcareous plankton record, *Marine*
948 *Micropaleontology*, 37, 1-22, 1999.

949 Flores, J. A. and Sierro, F. J.: Revised technique for calculation of calcareous nannofossil
950 accumulation rates, *Micropaleontology*, 43, 321-324, 1997.

- 951 Fryxell, G. A. and Hasle, G. R.: *Thalassiosira eccentrica* (Ehreb.) Cleve, *T. symmetrica*
952 sp. nov., and some related centric diatoms, *Journal of Phycology*, 8, 297-317, 1972.
- 953 Glushkova, O. Y.: Geomorphological correlation of Late Pleistocene glacial complexes
954 of Western and Eastern Beringia, *Quaternary Science Reviews*, 20, 405-417, 2001.
- 955 Gualtieri, L. and Brigham-Grette, J.: The age and origin of the Little Diomedede Island
956 upland surface, *Arctic*, 54, 12-21, 2001.
- 957 Gualtieri, L., Glushkova, O., and Brigham-Grette, J.: Evidence for restricted ice extent
958 during the last glacial maximum in the Koryak Mountains of Chukotka, far eastern
959 Russia, *Geological Society of America Bulletin*, 112, 1106-1118, 2000.
- 960 Håkansson, H.: A compilation and evaluation of species in the general *Stephanodiscus*,
961 *Cyclostephanos*, and *Cyclotella* with a new genus in the family Stephanodiscaceae,
962 *Diatom Research*, 17, 1-139, 2002.
- 963 Hall, I. R., McCave, L. N., Shackleton, N. J., Weedon, G. P., and Harris, S. E.:
964 Intensified deep Pacific inflow and ventilation in Pleistocene glacial times, *Nature*, 412,
965 809-812, 2001.
- 966 Hasle, G. R. and Heimdal, B. R.: Morphology and distribution of the marine centric
967 diatom *Thalassiosira antarctica* Comber, *Journal of the Royal Microscopical Society*, 88,
968 357-369, 1968.
- 969 Hay, M. B., Dallimore, A., Thomson, R. E., Calvert, S. E., and Pienitz, R.: Siliceous
970 microfossil record of late Holocene oceanography and climate along the west coast of
971 Vancouver Island, British Columbia (Canada), *Quaternary Research*, 67, 33-49, 2007.
- 972 Heiser, P. A. and Roush, J. J.: Pleistocene glaciations in Chukotka, Russia: moraine
973 mapping using satellite synthetic aperture radar (SAR) imagery, *Quaternary Science*
974 *Reviews*, 20, 393-404, 2001.

- 975 Hopkins, D. M.: Cenozoic Hhistory of the Bering Land Bridge, *Science*, 129, 1519-1528,
976 1959.
- 977 Hopkins, D. M.: The paleogeography and climatic history of Beringia during late
978 Cenozoic Time, *Internord*, 12, 121-150, 1972.
- 979 Hopkins, D. M.: Pleistocene glaciation on St. George, Pribilof Islands, *Science*, 1966.
980 343-345, 1966.
- 981 Horner, R.: *Sea Ice Biota*, CRC Press, Inc, Boca Raton, FL, 1985.
- 982 Hu, A. X., Meehl, G. A., Otto-Bliesner, B. L., Waelbroeck, C., Han, W. Q., Loutre, M.
983 F., Lambeck, K., Mitrovica, J. X., and Rosenbloom, N.: Influence of Bering Strait flow
984 and North Atlantic circulation on glacial sea-level changes, *Nature Geoscience*, 3, 118-
985 121, 2010.
- 986 Huston, M. M., Brigham-Grette, J., and Hopkins, D. M.: Paleogeographic significance of
987 middle Pleistocene glaciomarine deposits on Baldwin Peninsula, northwestern Alaska,
988 *Annals of Glaciology*, 14, 111-114, 1990.
- 989 IPCC: *Climate Change 2013: The Physical Science Basis. Contribution of Working*
990 *Group I to the Fifth Assessment Report of the Intergovernmental Panel on Climate*
991 *Change*. Stocker, T. F., Qin, D., Plattner, G.-K., Tignor, M., Allen, S. K., Boschung, J.,
992 Nauels, A., Xia, Y., Bex, V., and Midgley, P. M. (Eds.), Cambridge University Press,
993 Cambridge, U.K. and New York, NY, USA, 2013.
- 994 Iwasaki, S., Takahashi, K., Kanematsu, Y., Asahi, H., Onodera, J., and Ravelo, A. C.:
995 Paleoproductivity and paleoceanography of the last 4.3 Myrs at IODP Expedition 323
996 Site U1341 in the Bering Sea based on biogenic opal content, *Deep Sea Research Part II:*
997 *Topical Studies in Oceanography*, 125–126, 145-154, 2016.

998 Kandiano, E. S., Bauch, H. A., Fahl, K., Helmke, J. P., Roehl, U., Perez-Folgado, M., and
999 Cacho, I.: The meridional temperature gradient in the eastern North Atlantic during MIS
1000 11 and its link to the ocean-atmosphere system, *Palaeogeography Palaeoclimatology*
1001 *Palaeoecology*, 333, 24-39, 2012.

1002 Kanematsu, Y., Takahashi, K., Kim, S., Asahi, H., and Khim, B.-K.: Changes in biogenic
1003 opal productivity with Milankovitch cycles during the last 1.3 Ma at IODP Expedition
1004 323 Sites U1341, U1343, and U1345 in the Bering Sea, *Quaternary International*, 310,
1005 213-220, 2013.

1006 Kariya, C., Hyodo, M., Tanigawa, K., and Sato, H.: Sea-level variation during MIS 11
1007 constrained by stepwise Osaka Bay extensions and its relation with climatic evolution,
1008 *Quaternary Science Reviews*, 29, 1863-1879, 2010.

1009 Kato, Y., Onodera, J., Suto, I., Teraishi, A., and Takahashi, K.: Pliocene and Pleistocene
1010 paleoceanography in the western subarctic Pacific based on diatom analyses of ODP Leg
1011 145 Hole 884B and IODP Expedition 323 Holes U1341B and U1343E, *Deep Sea*
1012 *Research Part II: Topical Studies in Oceanography*, 125–126, 29-37, 2016.

1013 Katsuki, K. and Takahashi, K.: Diatoms as paleoenvironmental proxies for seasonal
1014 productivity, sea-ice and surface circulation in the Bering Sea during the late Quaternary,
1015 *Deep Sea Research II*, 52, 2110-2130, 2005.

1016 Kaufman, D., Young, N. E., Briner, J. P., and Manley, W. F.: Alaska Palaeo-Glacier
1017 Atlas (Version 2). In: *Developments in Quaternary Science*, Ehlers, J., Gibbard, P. L.,
1018 and Hughes, P. D. (Eds.), Amsterdam, The Netherlands, 2011.

1019 Kaufman, D. S.: Aminostratigraphy of Pliocene-Pleistocene high-sea-level deposits,
1020 Nome coastal plain and adjacent nearshore area, Alaska, *Geological Society of America*
1021 *Bulletin*, 104, 40-52, 1992.

- 1022 Kaufman, D. S. and Brigham-Grette, J.: Aminostratigraphic correlations and
1023 paleotemperature implications, Pliocene-Pleistocene high sea-level deposits,
1024 Northwestern Alaska, *Quaternary Science Reviews*, 12, 21-33, 1993.
- 1025 Kaufman, D. S., Manley, W. F., Forman, S. L., and Layer, P. W.: Pre-Late-Wisconsin
1026 glacial history, coastal Ahklun Mountains, southwestern Alaska - new amino acid,
1027 thermoluminescence, and $^{40}\text{Ar}/^{39}\text{Ar}$ results, *Quaternary Science Reviews*, 20, 337-352,
1028 2001.
- 1029 Kaufman, D. S., Walter, R. C., Brigham-Grette, J., and Hopkins, D. M.: Middle
1030 Pleistocene age of the Nome River glaciation, northwestern Alaska, *Quaternary*
1031 *Research*, 36, 277-293, 1991.
- 1032 Keigwin, L. D., Donnelly, J. P., Cook, M. S., Driscoll, N. W., and Brigham-Grette, J.:
1033 Rapid sea-level rise and Holocene climate in the Chukchi Sea, *Geology*, 34, 861-864,
1034 2006.
- 1035 Kim, S., Khim, B.-K., and Takahashi, K.: Late Pliocene to early Pleistocene (2.4–1.25
1036 Ma) paleoproductivity changes in the Bering Sea: IODP expedition 323 Hole U1343E,
1037 *Deep Sea Research Part II: Topical Studies in Oceanography*, 125–126, 155-162, 2016.
- 1038 Kim, S., Khim, B. K., and Goo Cho, H.: Clay mineral stratigraphy during the last 2.4 Ma
1039 at IODP Exp. 323 Site U1343 in the Bering Sea, *Marine Geology*, 359, 163-168, 2015.
- 1040 Kindler, P. and Hearty, P. J.: Elevated marine terraces from Eleuthera (Bahamas) and
1041 Bermuda: sedimentological, petrographic, and geochronological evidence for important
1042 deglaciation events during the middle Pleistocene, *Global and Planetary Change*, 24, 41-
1043 58, 2000.
- 1044 Kleinen, T., Hildebrandt, S., Prange, M., Rachmayani, R., Mueller, S., Bezrukova, E.,
1045 Brovkin, V., and Tarasov, P. E.: The climate and vegetation of Marine Isotope Stage 11-

- 1046 Model results and proxy-based reconstructions at global and regional scale, Quaternary
1047 International, 348, 247-265, 2014.
- 1048 Knudson, K. P. and Ravelo, A. C.: North Pacific Intermediate Water circulation enhanced
1049 by the closure of the Bering Strait, Paleoceanography, 30, 1287-1304, 2015.
- 1050 Koizumi, I.: The Late Cenozoic diatoms of Sites 183-193, Leg 19 Deep Sea Drilling
1051 Project, Initial Reports of the Deep Sea Drilling Project, 19, 805-855, 1973.
- 1052 Kowalik, Z.: Bering Sea Tides. In: Dynamics of the Bering Sea, Loughlin, T. R. and
1053 Ohtani, K. (Eds.), Universtiy of Alaska Sea Grant, Fairbanks, AK, 1999.
- 1054 Lisiecki, L. E. and Raymo, M. E.: A Pliocene-Pleistocene stack of 57 globally distributed
1055 benthic delta O-18 records, Paleoceanography, 20, 10.1029/2004PA001071, 2005.
- 1056 Liu, Z. H., Altabet, M. A., and Herbert, T. D.: Glacial-interglacial modulation of eastern
1057 tropical North Pacific denitrification over the last 1.8-Myr, Geophysical Research Letters,
1058 32, 2005.
- 1059 Lopes, C., Mix, A. C., and Abrantes, F.: Diatoms in northeast Pacific surface sediments
1060 as paleoceanographic proxies, Marine Micropaleontology, 60, 45-65, 2006.
- 1061 Loutre, M. F. and Berger, A.: Marine Isotope Stage 11 as an analogue for the present
1062 interglacial, Global and Planetary Change, 36, 209-217, 2003.
- 1063 Lozhkin, A. V. and Anderson, P.: Vegetation responses to interglacial warming in the
1064 Arctic: examples from Lake El'gygytgyn, Far East Russian Arctic, Clim Past, 9, 1211-
1065 1219, 2013.
- 1066 Lundholm, N. and Hasle, G. R.: Are *Fragilariopsis cylindrus* and *Fragilariopsis nana*
1067 bipolar diatoms? Morphological and molecular analyses of two sympatric species, Nova
1068 Hedwigia, 133, 231-250, 2008.

- 1069 Lundholm, N. and Hasle, G. R.: *Fragilariopsis* (Bacillariophyceae) of the Northern
1070 Hemisphere--morphology, taxonomy, phylogeny and distribution, with a description of
1071 *F. pacifica* sp. nov., *Phycologia*, 49, 438-460, 2010.
- 1072 Lyle, M., Heusser, L., Herbert, T., Mix, A. C., and Barron, J.: Interglacial theme and
1073 variations: 500 k.y. of orbital forcing and associated responses from the terrestrial and
1074 marine biosphere, U.S. Pacific Northwest, *Geology*, 29, 1115-1118, 2001.
- 1075 Manley, W. F.: Digital Elevation Model (DEM) for the Bering Land Bridge, INSTAAR,
1076 University of Colorado, Boulder, CO, 2002.
- 1077 Maurer, B. A. and McGill, B. J.: Chapter 5: measurement of species diversity. In:
1078 Biological Diversity, Magurran, A. E. and McGill, B. J. (Eds.), Oxford University Press,
1079 New York, 2011.
- 1080 McKay, R., Naish, T., Powell, R., Barrett, P., Scherer, R., Talarico, F., Kyle, P., Monien,
1081 D., Kuhn, G., Jackolski, C., and Williams, T.: Pleistocene variability of Antarctic Ice
1082 Sheet extent in the Ross Embayment, *Quaternary Science Reviews*, 34, 93-112, 2012.
- 1083 McManus, J., Oppo, D. W., Cullen, J. L., and Healey, S.: Marine Isotope Stage 11 (MIS
1084 11): analog for Holocene and future climate. In: Earth's Climate and Orbital Eccentricity:
1085 The Marine Isotope Stage 11, Droessler, A. W., Poore, R. Z., and Burkle, L. H. (Eds.),
1086 Geophysical Monograph 137, American Geophysical Union, Washington, DC, 2003.
- 1087 McQuoid, M. R. and Hobson, L. A.: A Holocene record of diatom and silicoflagellate
1088 microfossils in sediments of Saanich Inlet, ODP Leg 169S, *Marine Geology*, 174, 111-
1089 123, 2001.
- 1090 Medlin, L. K. and Hasle, G. R.: Some *Nitzschia* and related diatom species from fast ice
1091 samples in the Arctic and Antarctic, *Polar Biology*, 10, 451-479, 1990.

- 1092 Medlin, L. K. and Priddle, J.: Polar Marine Diatoms, British Antarctic Survey, Natural
1093 Environment Research Council, Cambridge, 1990.
- 1094 Melles, M., Brigham-Grette, J., Minyuk, P., Nowaczyk, N. R., Wennrich, V., DeConto,
1095 R. M., Anderson, P. M., Andreev, A. A., Coletti, A., Cook, T. L., Haltia-Hovi, E.,
1096 Kukkonen, M., Lozhkin, A. V., Rosen, P., Tarasov, P. E., Vogel, H., and Wagner, B.: 2.8
1097 Million years of Arctic climate change from Lake El'gygytyn, NE Russia, *Science*,
1098 2012. 2012.
- 1099 Meyers, P. A.: Preservation of elemental and isotopic source identification of
1100 sedimentary organic matter, *Chemical Geology*, 114, 289-302, 1994.
- 1101 Milker, Y., Rachmayani, R., Weinkauff, M. F. G., Prange, M., Raitzsch, M., Schulz, M.,
1102 and Kucera, M.: Global and regional sea surface temperature trends during Marine
1103 Isotope Stage 11, *Clim Past*, 9, 2231-2252, 2013.
- 1104 Miller, G. H., Brigham-Grette, J., Anderson, L., Bauch, H. A., Douglas, M. A., Edwards,
1105 M. E., Elias, S. A., Finney, B. P., Funder, S., Herbert, T., Hinzman, L. D., Kaufman, D.
1106 K., MacDonald, G. M., Robock, A., Serreze, M. C., Smol, J. P., Spielhagen, R. F., Wolfe,
1107 A. P., and Wolff, E. W.: Temperature and precipitation history of the Arctic. In: *Past
1108 Climate Variability and Change in the Arctic and at High Latitudes*, Research, U. S. C. C.
1109 P. a. S. o. G. C. (Ed.), U.S. Geological Survey, Reston, VA, 2009.
- 1110 Miller, G. H. and De Vernal, A.: Will greenhouse warming lead to Northern Hemisphere
1111 ice-sheet growth?, *Nature*, 355, 244-246, 1992.
- 1112 Muller, P. J.: C-N Ratios in Pacific Deep-Sea Sediments - Effect of Inorganic
1113 Ammonium and Organic Nitrogen Compounds Sorbed by Clays, *Geochimica Et
1114 Cosmochimica Acta*, 41, 765-776, 1977.
- 1115 Naish, T., Powell, R., Levy, R., Wilson, G., Scherer, R., Talarico, F., Krissek, L.,
1116 Niessen, F., Pompilio, M., Wilson, T., Carter, L., DeConto, R., Huybers, P., McKay, R.,

- 1117 Pollard, D., Ross, J., Winter, D., Barrett, P., Browne, G., Cody, R., Cowan, E., Crampton,
1118 J., Dunbar, G., Dunbar, N., Florindo, F., Gebhardt, C., Graham, I., Hannah, M., Hansaraj,
1119 D., Harwood, D., Helling, D., Henrys, S., Hinnov, L., Kuhn, G., Kyle, P., Laufer, A.,
1120 Maffioli, P., Magens, D., Mandernack, K., McIntosh, W., Millan, C., Morin, R.,
1121 Ohneiser, C., Paulsen, T., Persico, D., Raine, I., Reed, J., Riesselman, C., Sagnotti, L.,
1122 Schmitt, D., Sjunneskog, C., Strong, P., Taviani, M., Vogel, S., Wilch, T., and Williams,
1123 T.: Obliquity-paced Pliocene West Antarctic ice sheet oscillations, *Nature*, 458, 322-
1124 U384, 2009.
- 1125 Normack, W. R. and Carlson, P. R.: Giant submarine canyons: is size any clue to their
1126 importance in the rock record? In: Geological Society of America Special Paper, Chan,
1127 M. A. and Archer, A. W. (Eds.), Geological Society of America, Boulder, CO, 2003.
- 1128 Nürnberg, D., Wollenburg, I., Dethleff, D., Eicken, H., Kassens, H., Letzig, T., Reimnitz,
1129 E., and Thiede, J.: Sediments in Arctic Sea-Ice - Implications for Entrainment, Transport
1130 and Release, *Marine Geology*, 119, 185-214, 1994.
- 1131 Onodera, J. and Takahashi, K.: Diatoms and siliceous flagellates (silicoflagellates,
1132 ebridians, and endoskeletal dinoflagellate *Actiniscus*) from the Subarctic Pacific,
1133 *Memoirs of the Faculty of Sciences Kyushu University.*, Series D, Earth and Planetary
1134 Sciences, 31, 105-136, 2007.
- 1135 Onodera, J., Takahashi, K., and Nagatomo, R.: Diatoms, silicoflagellates, and ebridians at
1136 Site U1341 on the western slope of Bowers Ridge, IODP Expedition 323, *Deep Sea*
1137 *Research Part II: Topical Studies in Oceanography*, 125–126, 8-17, 2016.
- 1138 Ortiz, J. D., Nof, D., Polyak, L., St-Onge, G., Lisé-Pronovost, A., Naidu, S., Darby, D.,
1139 and Brachfeld, S.: The Late Quaternary Flow through the Bering Strait Has Been Forced
1140 by the Southern Ocean Winds, *Journal of Physical Oceanography*, 42, 2014-2029, 2012.
- 1141 PAGES, P. I. W. G. o., Berger, A., Crucifix, M., Hodell, D. A., Mangili, C., McManus, J.
1142 F., Otto-Bliesner, B., Pol, K., Raynaud, D., Skinner, L. C., Tzedakis, P. C., Wolff, E. W.,

- 1143 Yin, Q. Z., Abe-Ouchi, A., Barbante, C., Brovkin, V., Cacho, I., Capron, E., Ferretti, P.,
1144 Ganopolski, A., Grimalt, J. O., Hoenisch, B., Kawamura, K., Landais, A., Margari, V.,
1145 Martrat, B., Masson-Delmotte, V., Mokeddem, Z., Parrenin, F., Prokopenko, A. A.,
1146 Rashid, H., Schulz, M., and Riveiros, N. V.: Interglacials of the last 800,000years, *Rev*
1147 *Geophys*, 54, 162-219, 2016.
- 1148 Perdue, E. M. and Koprivnjak, J.-F.: Using the C/N ratio to estimate terrigenous inputs of
1149 organic matter to aquatic environments, *Estuar Coast Shelf S*, 73, 65-72, 2007.
- 1150 Pol, K.: Links between MIS 11 millennial to sub-millennial climate variability and long
1151 term trends as revealed by new high resolution EPICA Dome C deuterium data - A
1152 comparison with the Holocene, *Clim Past*, 7, 437-450, 2011.
- 1153 Poli, M. S., Meyers, P. A., and Thunell, R. C.: The western North Atlantic record of MIS
1154 13 to 10: Changes in primary productivity, organic carbon accumulation and benthic
1155 foraminiferal assemblages in sediments from the Blake Outer Ridge (ODP Site 1058),
1156 *Palaeogeography, Palaeoclimatology, Palaeoecology*, 295, 89-101, 2010.
- 1157 Pollard, D. and DeConto, R. M.: Modelling West Antarctic ice sheet growth and collapse
1158 through the past five million years, *Nature*, 458, 329-U389, 2009.
- 1159 Prokopenko, A. A., Bezrukova, E. V., Khursevich, G. K., Solotchina, E. P., Kuzmin, M.
1160 I., and Tarasov, P. E.: Climate in continental interior Asia during the longest interglacial
1161 of the past 500 000 years: the new MIS 11 records from Lake Baikal, SE Siberia, *Clim*
1162 *Past*, 6, 31-48, 2010.
- 1163 Pushkar, V. S., Roof, S. R., Cherepanova, M. V., Hopkins, D. M., and Brigham-Grette,
1164 J.: Paleogeographic and paleoclimatic significance of diatoms from Middle Pleistocene
1165 marine and glaciomarine deposits on Baldwin Peninsula, northwestern Alaska,
1166 *Palaeogeography, Palaeoclimatology, Palaeoecology*, 152, 67-85, 1999.

- 1167 Raymo, M. E. and Mitrovica, J. X.: Collapse of polar ice sheets during the stage 11
1168 interglacial, *Nature*, 483, 453-456, 2012.
- 1169 Raymo, M. E., Mitrovica, J. X., O'Leary, M. J., DeConto, R. M., and Hearty, P. J.:
1170 Departures from eustasy in Pliocene sea-level records, *Nature Geoscience*, 4, 328-332,
1171 2011.
- 1172 Raynaud, D., Barnola, J. M., Souchez, R., Lorrain, R., Petit, J. R., Duval, P., and
1173 Lipenkov, V. Y.: The record for Marine Isotopic Stage 11, *Nature*, 436, 39-40, 2005.
- 1174 Redfield, A. C., Ketchum, B. H., and Richards, F. A.: The influence of organisms on the
1175 composition of sea water. In: *The Sea*, Hill, M. N. (Ed.), Wiley, New York, 1963.
- 1176 Reimnitz, E., McCormick, M., Bischof, J., and Darby, D. A.: Comparing sea-ice
1177 sediment load with Beaufort Sea shelf deposits: is entrainment selective?, *Journal of*
1178 *Sedimentary Research*, 68, 777-787, 1998.
- 1179 Reyes, A. V., Carlson, A. E., Beard, B. L., Hatfield, R. G., Stoner, J. S., Winsor, K.,
1180 Welke, B., and Ullman, D. J.: South Greenland ice-sheet collapse during Marine Isotope
1181 Stage 11, *Nature*, 510, 525-+, 2014.
- 1182 Rohling, E. J., Braun, K., Grant, K., Kucera, M., Roberts, A. P., Siddall, M., and
1183 Trommer, G.: Comparison between Holocene and Marine Isotope Stage-11 sea-level
1184 histories, *Earth and Planetary Science Letters*, 291, 97-105, 2010.
- 1185 Rohling, E. J., Foster, G. L., Grant, K. M., Marino, G., Roberts, A. P., Tamisiea, M. E.,
1186 and Williams, F.: Sea-level and deep-sea-temperature variability over the past 5.3 million
1187 years (vol 508, pg 477, 2014), *Nature*, 510, 432-432, 2014.
- 1188 Saito, K. and Taniguchi, A.: Phytoplankton communities in the Bering Sea and adjacent
1189 seas II: spring and summer communities in seasonally ice-covered areas, *Astarte*, 11, 27-
1190 35, 1978.

- 1191 Sancetta, C. A.: Distribution of diatom species in surface sediments of the Bering and
1192 Okhotsk seas, *Micropaleontology*, 28, 221-257, 1982.
- 1193 Sancetta, C. A.: Oceanographic and ecologic significance of diatoms in surface sediments
1194 of the Bering and Okhotsk seas, *Deep Sea Research*, 28A, 789-817, 1981.
- 1195 Sancetta, C. A.: Three species of *Coscinodiscus* Ehrenberg from North Pacific sediments
1196 examined in the light and scanning electron microscopes, *Micropaleontology*, 33, 230-
1197 241, 1987.
- 1198 Sancetta, C. A. and Robinson, S. W.: Diatom evidence on Wisconsin and Holocene
1199 events in the Bering Sea, *Quaternary Research*, 20, 232-245, 1983.
- 1200 Sancetta, C. A. and Silvestri, S. M.: Pliocene-Pleistocene evolution of the North Pacific
1201 ocean-atmosphere system, interpreted from fossil diatoms, *Paleoceanography*, 1, 163-
1202 180, 1986.
- 1203 Schandelmeier, L. and Alexander, V.: An analysis of the influence of ice on spring
1204 phytoplankton population structure in the southeast Bering Sea, *Limnology and*
1205 *Oceanography*, 26, 935-943, 1981.
- 1206 Scherer, R. P.: A new method for the determination of absolute abundance of diatoms
1207 and other silt-sized sedimentary particles, *Journal of Paleolimnology*, 12, 171-179, 1994.
- 1208 Scherer, R. P., Aldahan, A., Tulaczyk, S., Possnert, G., Engelhardt, H., and Kamb, B.:
1209 Pleistocene collapse of the West Antarctic Ice Sheet, *Science*, 281, 82-85, 1998.
- 1210 Schlung, S. A., Ravelo, A. C., Aiello, I. W., Andreasen, D. H., Cook, M. S., Drake, M.,
1211 Dyez, K. A., Guilderson, T. P., LaRiviere, J. P., Stroynowski, Z., and Takahashi, K.:
1212 Millennial-scale climate change and intermediate water circulation in the Bering Sea
1213 from 90 ka: A high-resolution record from IODP Site U1340, *Paleoceanography*, 28,
1214 2013.

- 1215 Schrader, H. J. and Gersonde, R.: Diatoms and silicoflagellates. In: Micropaleontological
1216 counting methods and techniques - an exercise on an eight metres section of the Lower
1217 Pliocene of Capo Rossello, Sicily, Zachariasse, W. J., Riedel, W. R., Sanfilippo, A.,
1218 Schmidt, R. R., Brolsma, M. J., Schrader, H. J., Gersonde, R., Drooger, M. M., and
1219 Broekman, J. A. (Eds.), Utrecht Micropaleontological Bulletin, Netherlands, 1978.
- 1220 Schubert, C. J. and Calvert, S. E.: Nitrogen and carbon isotopic composition of marine
1221 and terrestrial organic matter in Arctic Ocean sediments: implications for nutrient
1222 utilization and organic matter composition, *Deep Sea Research I*, 48, 789-810, 2001.
- 1223 Schumacher, J. D. and Stabeno, P. J.: Continental shelf of the Bering Sea. In: *The sea*,
1224 Robinson, A. R. and Brink, K. H. (Eds.), John Wiley and Sons, New York, 1998.
- 1225 Shiga, K. and Koizumi, I.: Latest Quaternary oceanographic changes in the Okhotsk Sea
1226 based on diatom records, *Marine Micropaleontology*, 38, 91-117, 2000.
- 1227 Sigman, D., Altabet, M., Francois, R., McCorkle, D., and Gaillard, J.-F.: The isotopic
1228 composition of diatom-bound nitrogen in Southern Ocean sediments, *Paleoceanography*,
1229 14, 118-134, 1999.
- 1230 Smol, J. P.: The paleolimnologist's Rosetta Stone: calibrating indicators to environmental
1231 variables using surface-sediment training sets. In: *Pollution of lakes and rivers: a*
1232 *paleoenvironmental perspective*, Smol, J. P. (Ed.), Key issues in environmental change,
1233 Oxford University Press, New York, 2002.
- 1234 Springer, A. M., McRoy, C. P., and Flint, M. V.: The Bering Sea green belt: shelf edge
1235 processes and ecosystem production, *Fisheries Oceanography*, 5, 205-223, 1996.
- 1236 St. John, K.: Cenozoic ice-rafting history of the central Arctic Ocean: Terrigenous sands
1237 on the Lomonosov Ridge, *Paleoceanography*, 23, 10.1029/2007pa001483, 2008.

- 1238 Stabeno, P. J., Schumacher, J. D., and Ohtani, K.: The physical oceanography of the
1239 Bering Sea. In: Dynamics of the Bering Sea: a summary of physical, chemical, and
1240 biological characteristics, and a synopsis of research on the Bering Sea, Loughlin, T. R.
1241 and Ohtani, K. (Eds.), University of Alaska Sea Grant, Fairbanks, AK, 1999.
- 1242 Stroynowski, Z., Ravelo, A. C., and Andreasen, D.: A Pliocene to recent history of the
1243 Bering Sea at Site U1340A, IODP Expedition 323, *Paleoceanography*, 30, 1641-1656,
1244 2015.
- 1245 Syvertsen, E. E.: Resting Spore Formation in Clonal Cultures of *Thalassiosira antarctica*
1246 Comber, *T. nordenskiöldii* Cleve and *Detonula confervacea* (Cleve) Gran, *Nova*
1247 *Hedwigia*, 64, 41-63, 1979.
- 1248 Takahashi, K., Ravelo, A. C., Alvarez Zarikian, C. A., and Scientists, E.: Proceedings of
1249 the Integrated Ocean Drilling Program. Tokyo, 2011.
- 1250 Tarasov, P. E., Nakagawa, T., Demske, D., Österle, H., Igarashi, Y., Kitagawa, J.,
1251 Mokhova, L., Bazarova, V., Okuda, M., Gotanda, K., Miyoshi, N., Fujiki, T., Takemura,
1252 K., Yonenobu, H., and Fleck, A.: Progress in the reconstruction of Quaternary climate
1253 dynamics in the Northwest Pacific: A new modern analogue reference dataset and its
1254 application to the 430-kyr pollen record from Lake Biwa, *Earth-Science Reviews*, 108,
1255 64-79, 2011.
- 1256 Teitler, L., Florindo, F., Warnke, D. A., Filippelli, G. M., Kupp, G., and Taylor, B.:
1257 Antarctic Ice Sheet response to a long warm interval across Marine Isotope Stage 31: A
1258 cross-latitudinal study of iceberg-rafted debris, *Earth and Planetary Science Letters*, 409,
1259 109-119, 2015.
- 1260 Teraishi, A., Suto, I., Onodera, J., and Takahashi, K.: Diatom, silicoflagellate and
1261 ebridian biostratigraphy and paleoceanography in IODP 323 Hole U1343E at the Bering
1262 slope site, *Deep Sea Research Part II: Topical Studies in Oceanography*, 125–126, 18-28,
1263 2016.

- 1264 Ternois, Y., Kawamura, K., Keigwin, L., Ohkouchi, N., and Nakatsuka, T.: A biomarker
1265 approach for assessing marine and terrigenous inputs to the sediments of Sea of Okhotsk
1266 for the last 27,000 years, *Geochimica et Cosmochimica Acta*, 65, 791-802, 2001.
- 1267 Tomas, C. R.: *Identifying marine diatoms and dinoflagellates*, Academic Press, Inc.
1268 Harcourt Brace and Co., Boston, U.S.A., 1996.
- 1269 Tzedakis, P. C.: The MIS 11 – MIS 1 analogy, southern European vegetation,
1270 atmospheric methane and the “early anthropogenic hypothesis”, *Clim Past*, 6, 131-144,
1271 2010.
- 1272 van Hengstum, P. J., Scott, D. B., and Javaux, E. J.: Foraminifera in elevated Bermudian
1273 caves provide further evidence for +21m eustatic sea level during Marine Isotope Stage
1274 11, *Quaternary Science Reviews*, 28, 1850-1860, 2009.
- 1275 Voelker, A. H. L., Rodrigues, T., Billups, K., Oppo, D., McManus, J., Stein, R., Hefter,
1276 J., and Grimalt, J. O.: Variations in mid-latitude North Atlantic surface water properties
1277 during the mid-Brunhes (MIS 9–14) and their implications for the thermohaline
1278 circulation, *Clim Past*, 6, 531-552, 2010.
- 1279 Vogel, H., Meyer-Jacob, C., Melles, M., Brigham-Grette, J., Andreev, A. A., Wennrich,
1280 V., Tarasov, P. E., and Rosen, P.: Detailed insight into Arctic climatic variability during
1281 MIS 11c at Lake El'gygytgyn, NE Russia, *Clim Past*, 9, 1467-1479, 2013.
- 1282 von Quillfeldt, C. H.: Identification of some easily confused common diatom species in
1283 Arctic spring blooms, *Botanica Marina*, 44, 375-389, 2001.
- 1284 von Quillfeldt, C. H., Ambrose, W. G. J., and Clough, L. M.: High number of diatom
1285 species in first-year ice from the Chukchi Sea, *Polar Biology*, 26, 806-818, 2003.

- 1286 Walinsky, S. E., Prahl, F. G., Mix, A. C., Finney, B. P., Jaeger, J. M., and Rosen, G. P.:
1287 Distribution and composition of organic matter in surface sediments of coastal Southeast
1288 Alaska, *Continental Shelf Research*, 29, 1565-1579, 2009.
- 1289 Witkowski, A., Lange-Bertalot, H., and Metzeltin, D.: *Diatom Flora of Marine Coasts I*,
1290 A.R.G. Gantner Verlag K.G., Ruggell, Liechtenstein, 2000.
- 1291 Young, J. R., Geisen, M., Cros, L., Keleijne, A., Sprengel, C., Probert, I., and
1292 Østengaard, J.: A guide to extant coccolithophore taxonomy, *Journal of Nannoplankton*
1293 *Research*, Special Issue, 1, 1-125, 2003.
- 1294

1295 **Table 1:** Age-Depth Tie Points Used in the Age Model for U1345

1296

Depth (m CCSF-A)	Age (ka)	Date Type
98.6	337	Foraminifera {Cook, 2016}
115.3	374	Foraminifera {Cook, 2016}
123.2	398.5	Magnetic Susceptibility Correlation
130.6	424	Foraminifera {Cook, 2016}
148.7	478	Foraminifera {Cook, 2016}

1297

1298 **Table 2:** Depths and Ages of major climate intervals referred to in the text

Interval	Depth begin (m CCSF-A)	Depth end (m CCSF-A)	Begin (ka)	End (ka)
Late MIS 11/10	121.80	110.57	394	364
Beringian Glacial Initiation	124.94	121.80	405	394
Peak MIS 11	130.16	121.80	423	394
Termination V	131.09	130.16	425	423
MIS 12	133.10	131.09	431	425

1299

1300 Table 3: Bering Sea diatom species grouped by environmental niche. In cases where a species appears in more than one niche, the
 1301 grouping used in this study is highlighted in bold.

<i>Modern Seasonal Succession</i>			
Epontic	Marginal Ice Zone (MIZ)	Both Epontic and MIZ	Summer Bloom
<i>Navicula transitrans</i>	<i>Bacterosira bathyomphala</i>	<i>Actinocyclus curvatus</i>	<i>Coscinodiscus</i> spp.
<i>Synedropsis hyperborea</i>	<i>Chaetoceros furcellatus</i>	<i>Fossula arctica</i>	<i>Leptocylindrus</i> sp.
	<i>Chaetoceros socialis</i>	<i>Fragilariopsis cylindrus</i>	<i>Rhizosolenia</i> spp.
	<i>Leptocylindrus</i> sp.	<i>Fragilariopsis oceanica</i>	
	<i>Odontella aurita</i>	<i>Fragilariopsis regina-jahniae</i>	
	<i>Paralia sulcata</i>	<i>Navicula pelagica</i>	
	<i>Porosira glacialis</i>	Naviculoid pennates	
	<i>Staurosirella</i> cf. <i>pinnata</i>	<i>Nitzschia</i> spp.	
	<i>Thalassionema nitzschioides</i>	<i>Pinnularia quadratarea</i>	
	<i>Thalassiosira angulata</i>	<i>Thalassiosira antarctica</i> RS	
	<i>Thalassiosira baltica</i>	<i>Thalassiosira gravida</i>	
	<i>Thalassiosira decipiens</i>		
	<i>Thalassiosira hyalina</i>		
	<i>Thalassiosira hyperborea</i>		
	<i>Thalassiosira nordenskiöldii</i>		
	<i>Thalassiosira pacifica</i>		

1302 Continued on next page

Table 3 continued

<i>Water Mass Tracers</i>				<i>Shelf to Basin Transport</i>	
Dicothermal	High Productivity	Alaska Stream	Warmer Water	Neritic	Fresh Water
<i>Actinocyclus curvatulus</i>	<i>Chaetoceros</i> spp.	<i>Neodenticula seminae</i>	<i>Azpeitia tabularis</i>	<i>Actinoptychus senarius</i>	<i>Lindavia</i> cf. <i>ocellata</i>
<i>Shionodiscus trifultus</i>	<i>Odontella aurita</i>		<i>Stellarimia stellaris</i>	<i>Amphora</i> sp.	<i>Lindavia stylorum</i>
	<i>Thalassionema nitzschioides</i>		<i>Thalassionema nitzschioides</i>	<i>Lindavia stylorum</i>	<i>Staurosirella</i> cf. <i>pinnata</i>
	<i>Thalassiosira pacifica</i>		<i>Thalassiosira eccentrica</i>	<i>Delphineis</i> spp.	<i>Lindavia radiosa</i>
	<i>Thalassiosira</i> spp. small		<i>Shionodiscus oestrupii</i>	<i>Detonula confervacea</i>	
	<i>Thalassiothrix longissima</i>		<i>Thalassiosira symmetrica</i>	<i>Diploneis smithii</i>	
				Naviculoid pennates	
				<i>Odontella aurita</i>	
				<i>Paralia sulcata</i>	
				<i>Rhaphoneis ampiceros</i>	
				<i>Stephanopyxis turris</i>	
				<i>Thalassiosira angulata</i>	
				<i>Thalassiosira decipiens</i>	
				<i>Thalassiosira eccentrica</i>	

1304 **Table 4:** Distribution of Laminated Intervals during MIS 11. Note that the depth and age
 1305 of laminated intervals encompasses all holes drilled, but the median duration is
 1306 calculated using each of the holes that it is present in.

Lamination	Type	Depth (mbsf)	Age (ka)	Median Duration (kyrs)	Found in Holes
MIS 11.5	II	112.02-111.47	367.23-366.00	0.51	CDE
MIS 11.4	II	113.14-112.94	369.72-369.26	0.34	CD
MIS 11.3	II	114.28-113.95	372.25-371.52	0.73	D
MIS 11.2	II	115.59-114.69	374.75-373.17	1.23	ACE
MIS 11.1	II	121.84-121.18	394.12-392.09	1.10	CE
Termination V	I	130.23-126.51	423.28-410.44	12.04	ACDE

1307 **Table 5:** Summary Statistics for X-Ray Diffraction
 1308

	Mean	Standard	Minimum	Maximum
Full pattern degree of	0.257	0.014	0.242	0.282
Mineral	(wt.	(wt. %)	(wt. %)	(wt. %)
<i>Non-clays</i>				
Quartz	14	2	9	16
Kspar	1	1	0	2
Plag	9	2	5	12
Calcite	Tr	Tr	0	1
Aragonite	2	1	0	3
Dolomite	2	1	1	3
Siderite	1	1	0	2
Amphibole	4	1	3	5
Pyroxene	1	1	0	2
Pyrite	1	0	0	1
Magnetite	Tr	Tr	0	1
Hematite	Tr	Tr	0	1
Goethite	Tr	Tr	0	0
Maghemite	Tr	Tr	0	1
Titanite	1	1	0	3
Tephra	21	5	16	35
Zircon	Tr	Tr	0	0
<i>Total Non-clays</i>	57	2	54	63
<i>Clays</i>				
Kaolinite	0	0	0	0
Smectite	0	0	0	0
Illite	8	3	2	11
Biotite	2	1	0	3
Chlorite	33	3	29	38
Muscovite	Tr	1	0	2
<i>Total Clays</i>	43	2	37	46
Total	100			

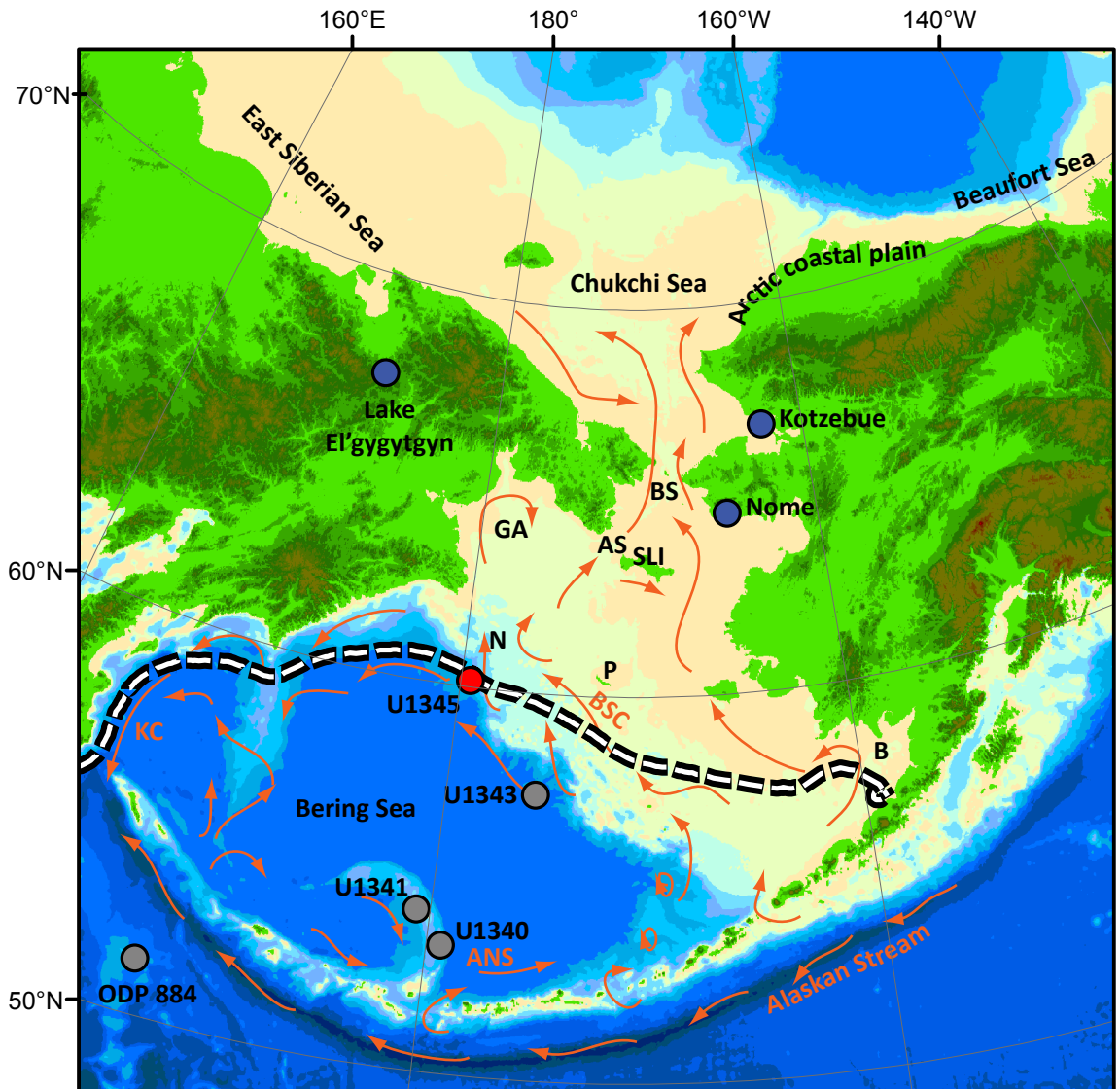


Figure 1. Map of Beringia with locations of cores mentioned in the text (U1345 (red dot), and U1340, U1341, U1343, and ODP Site 884 (grey dots)). Locations of place names from the text are labeled: Aleutian North Slope Current (ANS), Anadyr Strait (AS), Bristol Bay (B), Bering Strait (BS), Bering Slope Current (BSC), Gulf of Anadyr (GA), Kamchatka Current (KC), Navarin Canyon (N), Pribilof Islands (P), St. Lawrence Island (SLI). The white and black dashed line is the maximum extent of sea ice (median over the period 1979-2013) (Cavaliere et al., 1996). Currents are in orange and are modified from Stabeno (1999). Base map is modified from Manley (2002).

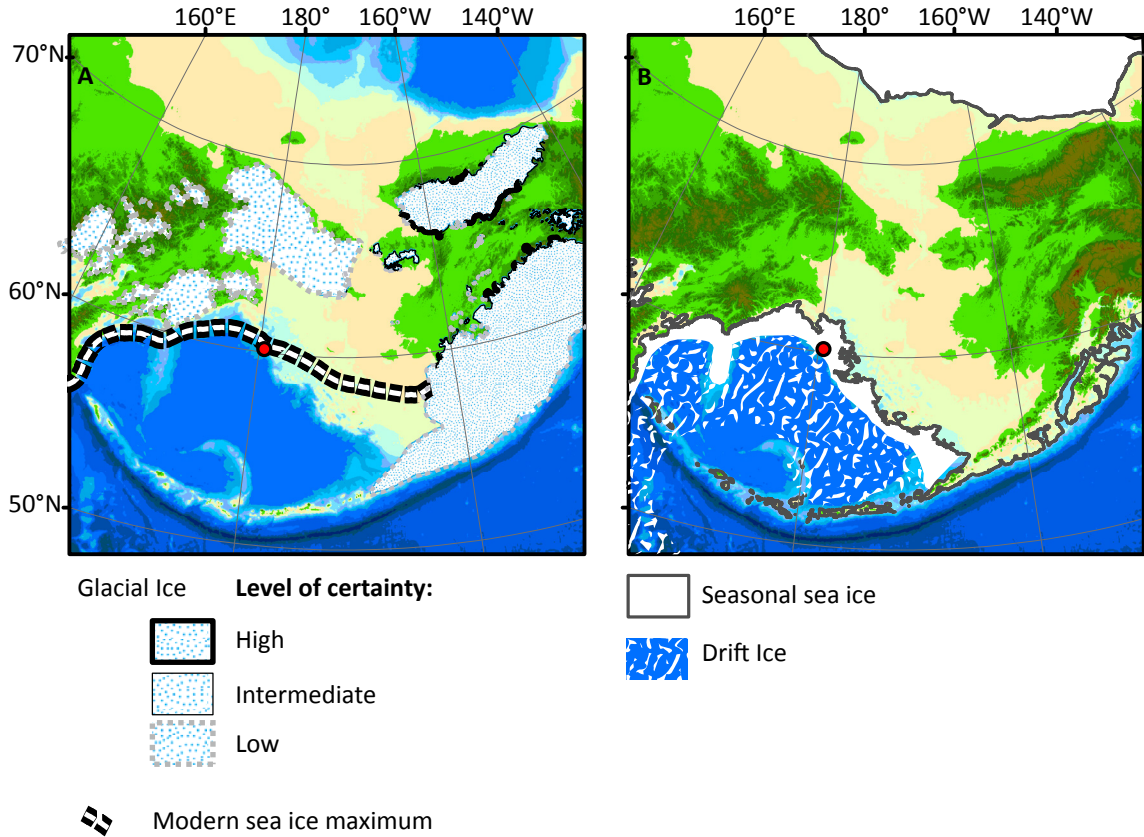


Figure 2. Maximum glacial and sea ice extents in Beringia. **A.** depicts the maximum glacial ice in Beringia as inferred from terminal and lateral moraines (Gaultieri et al., 2000; Heiser and Roush, 2001; Kaufman, et al., 2011; Barr and Clark, 2009). This is not intended to show the maximum extent during a particular glaciation, but rather the maximum possible extent of glacial ice. These moraines are likely from several different major glaciations. The level of certainty is indicated by the thickness of the line at the moraine. The white and black dashed line is the maximum extent of sea ice (median over period 1979-2013) (Cavalieri et al., 1996). **B.** depicts the approximate pattern of sea ice during glacial stages (Katsuki and Takahashi, 2005). The dark grey contour is -140 mapsl, the approximate sea level during MIS 12 (Rohling et al., 2010). Base map is modified from Manley (2002).

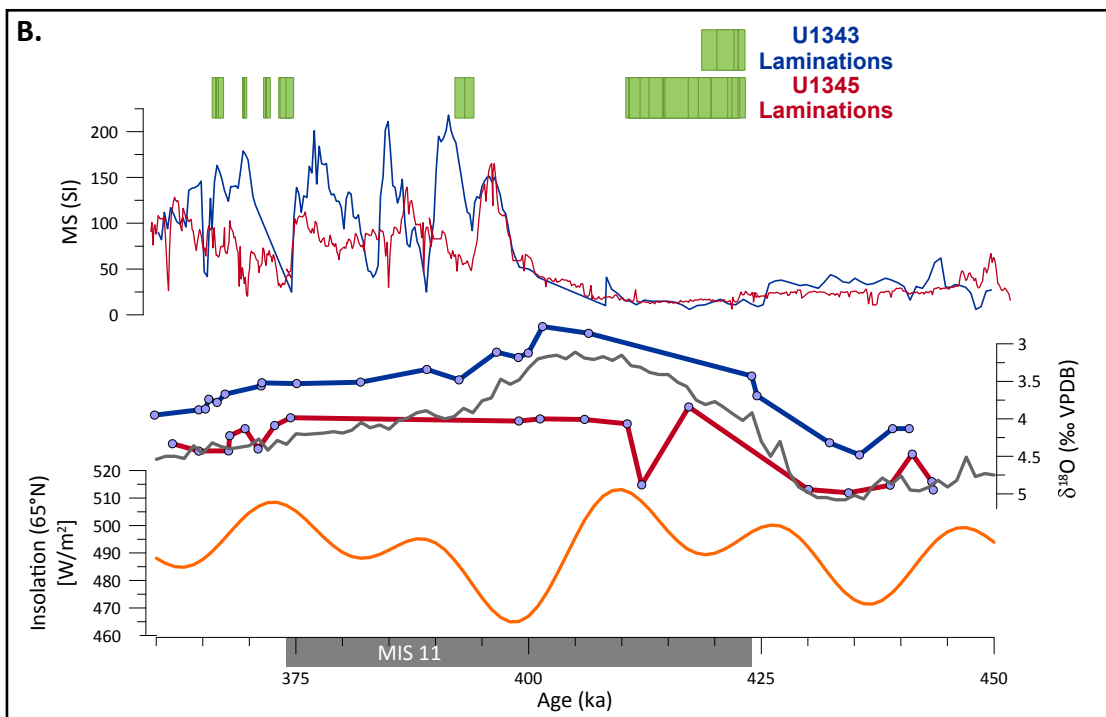
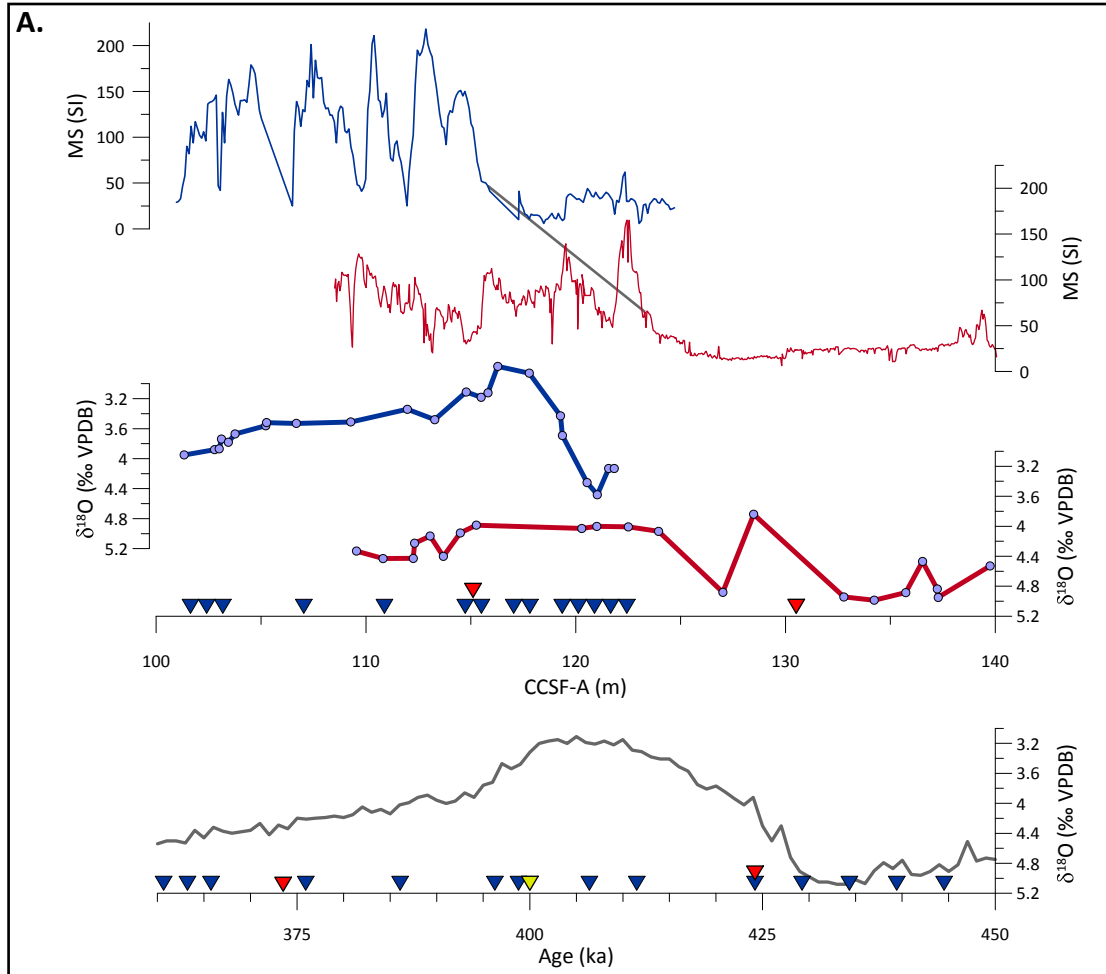


Figure 3.

1 **Figure 3A.** Age model plotted by depth. Blue plots depict data from Site U1343, red
2 plots are from U1345. Magnetic susceptibility and benthic foraminiferal $\delta^{18}\text{O}$ are plotted
3 by depth for each Site in the top half of the figure. The grey line joining the magnetic
4 susceptibility plots indicates the tie point that was added in this study. Inverted triangles
5 indicate locations of tie points (red: U1345, blue: U1343, grey: magnetic susceptibility)
6 between Bering Sea $\delta^{18}\text{O}$ (Cook et al., 2016; Asahi et al., 2016) and the global marine
7 stack (Lisiecki and Raymo, 2005), which is plotted in grey. **B:** Age model plotted by age.
8 Magnetic susceptibility and $\delta^{18}\text{O}$ are shown with the global marine $\delta^{18}\text{O}$ stack (grey) and
9 insolation at 65° N (orange). Green bars indicate laminated intervals in U1343 and
10 U1345.
11
12
13

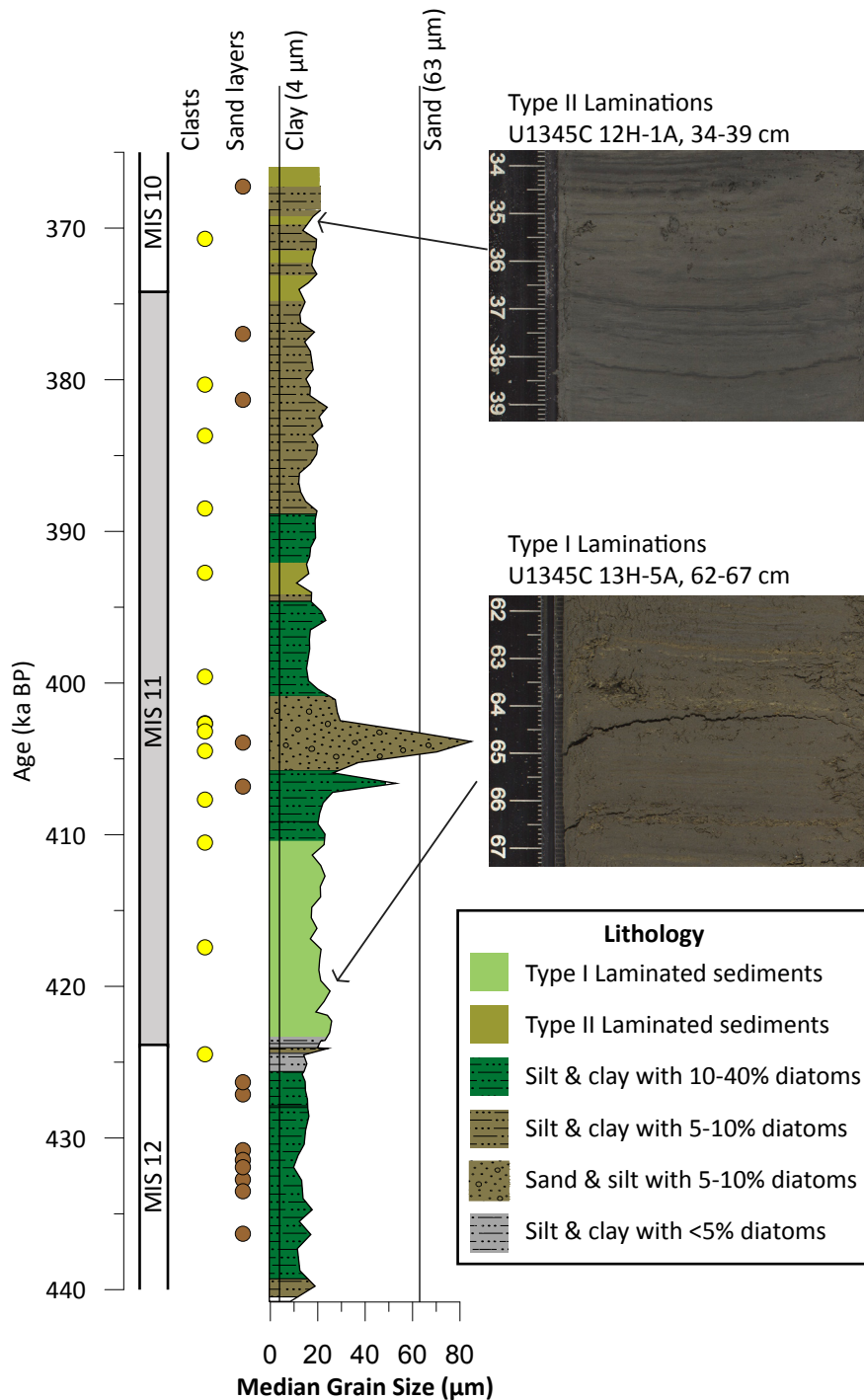


Figure 4. Lithostratigraphic column for U1345A. Marine Isotope Stage 11 is depicted as a grey bar. Ice rafted debris (yellow dots) and sand layers (maroon dots) are a compilation of these features in all four holes at U1345. The width of the lithologic column varies according to median grain size. Vertical lines indicate the cut off for clay and sand sized particles. Silt lies between the two lines. Colors depict varying amounts of diatoms relative to terrigenous grains in the sediment. Type I Laminations are depicted as pale green bars and Type II laminations are depicted as olive green bars. An example of each of the lamination types is shown in the images to the right.

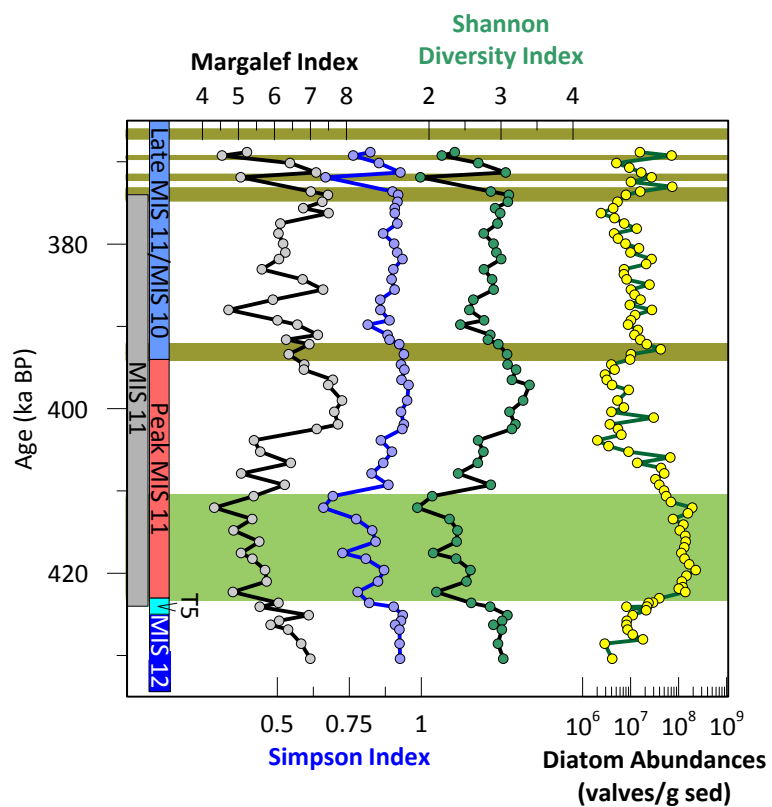


Figure 5. The Margalef, Simpson, and Shannon diversity indices plotted with diatom abundances. Type I Laminations are depicted as pale green bars and Type II laminations are depicted as olive green bars. Colored vertical bars refer to the zones mentioned in the text.

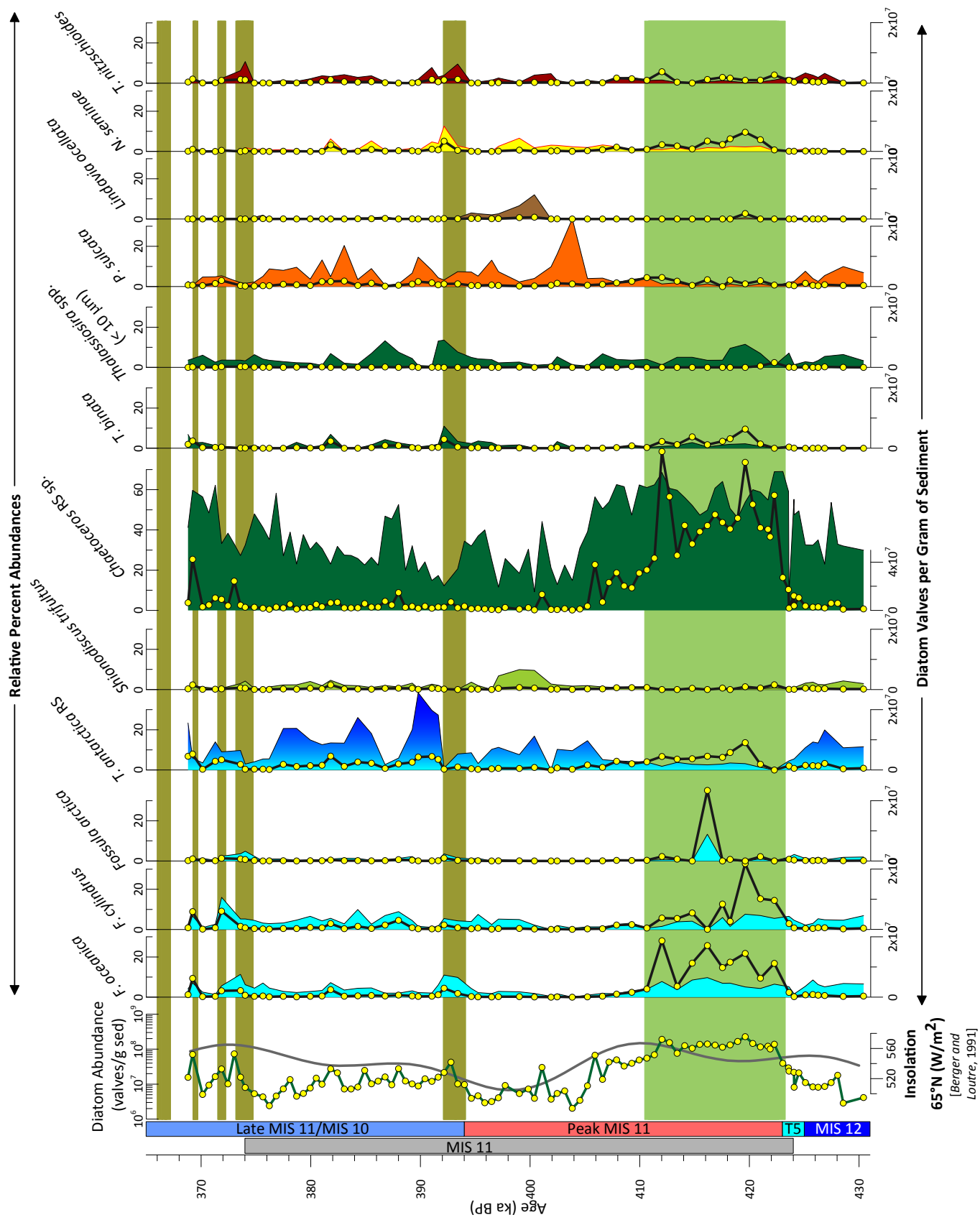


Figure 6.

14 **Figure 6.** Absolute and relative percent abundances of all diatoms that occur in
15 abundances greater than 10% of any assemblage. Colored vertical bars refer to the zones
16 mentioned in the text. Line plots depict absolute abundance and area plots depict relative
17 percent abundance. Species are color coded according to the niche that they are grouped
18 into: marginal ice zone (light blue), both ice types (dark blue to light blue), dicothermal
19 (light green), high productivity (green), neritic (orange), freshwater (brown), North
20 Pacific (yellow), and warm water (red). Insolation 65° N (light grey line) is also shown.
21 Type I Laminations are depicted as pale green bars and Type II laminations are depicted
22 as olive green bars.

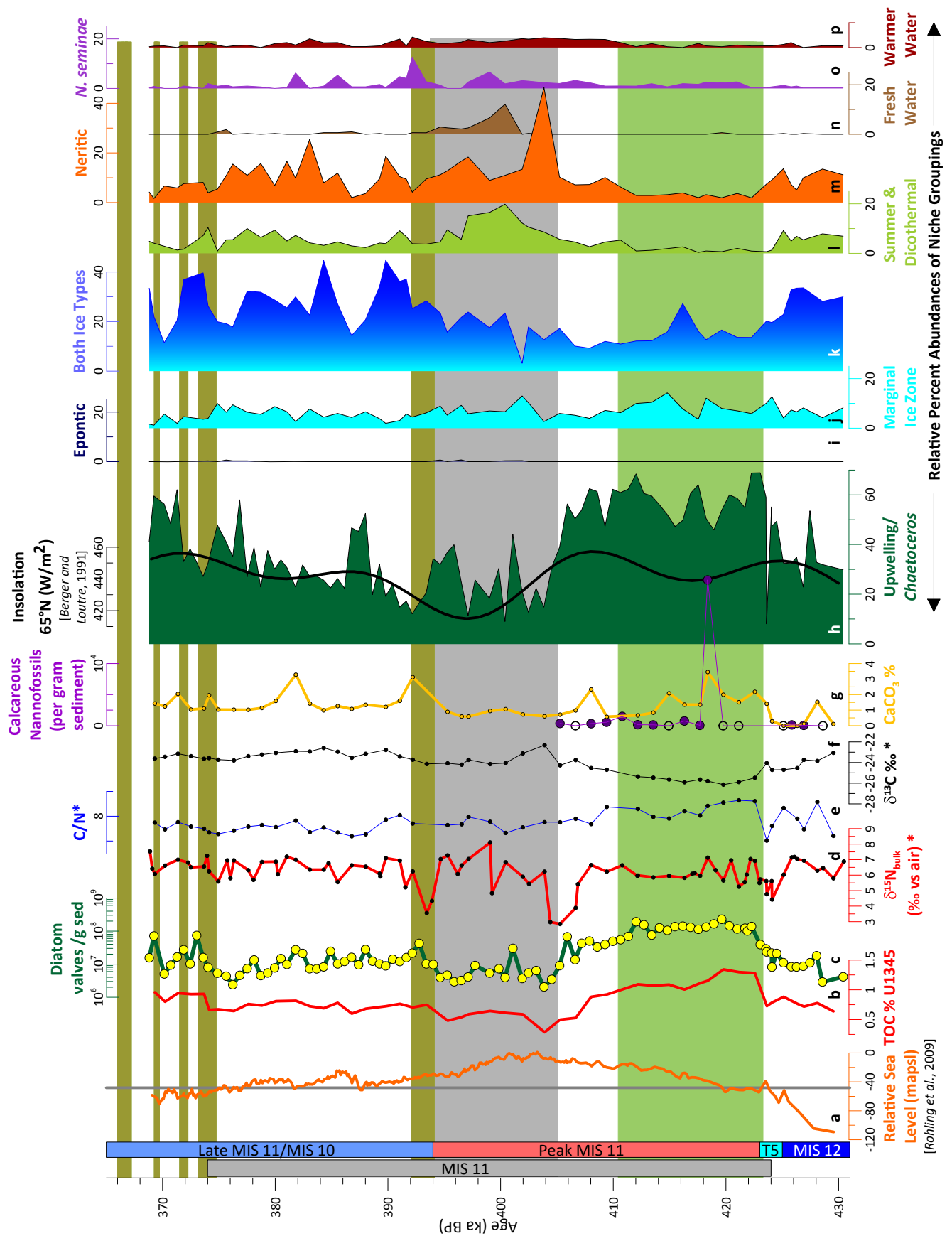


Figure 7.

23 **Figure 7.** Summary of geochemistry and biological proxies. The grey vertical bar depicts
24 the duration of MIS 11 and colored vertical bars refer to the zones mentioned in the text.
25 **A.** Global eustatic sea level (orange) is plotted for reference (Rohling et al., 2010). The
26 sill depth of Bering Strait (-50 m apsl) is shown as a vertical grey line. Total organic
27 carbon (**B.** red) is plotted with the total diatom abundance (**C.** green line, yellow dots).
28 Geochemical data is plotted as $\delta^{15}\text{N}$ (**D.** red), C/N (**E.** blue), $\delta^{13}\text{C}$ (**F.** black), and %
29 CaCO_3 (**G.** yellow). Biological proxies include absolute abundance of calcareous
30 nannofossils (**G.** purple). Open circles indicate barren samples; closed circles indicate
31 samples that had calcareous nannofossils present. Relative percent abundances of diatoms
32 are grouped by environmental niche. *Chaetoceros* RS are green (**H.**), epontic species are
33 navy blue (**I.**), marginal ice zone species are light blue (**J.**), species that fall under both
34 ice categories are shaded with a gradational blue (**K.**), summer and dicothermal species
35 are light green (**L.**), neritic species are orange (**M.**), fresh water species are brown (**N.**),
36 *N. seminae* is purple (**O.**), and warmer water species are maroon (**P.**). Insolation at 65° N
37 (black) is overlain on *Chaetoceros* RS relative percent abundances. Type I Laminations
38 are depicted as pale green bars and Type II laminations are depicted as olive green bars.
39 A grey bar indicates the Beringian glacial advance.

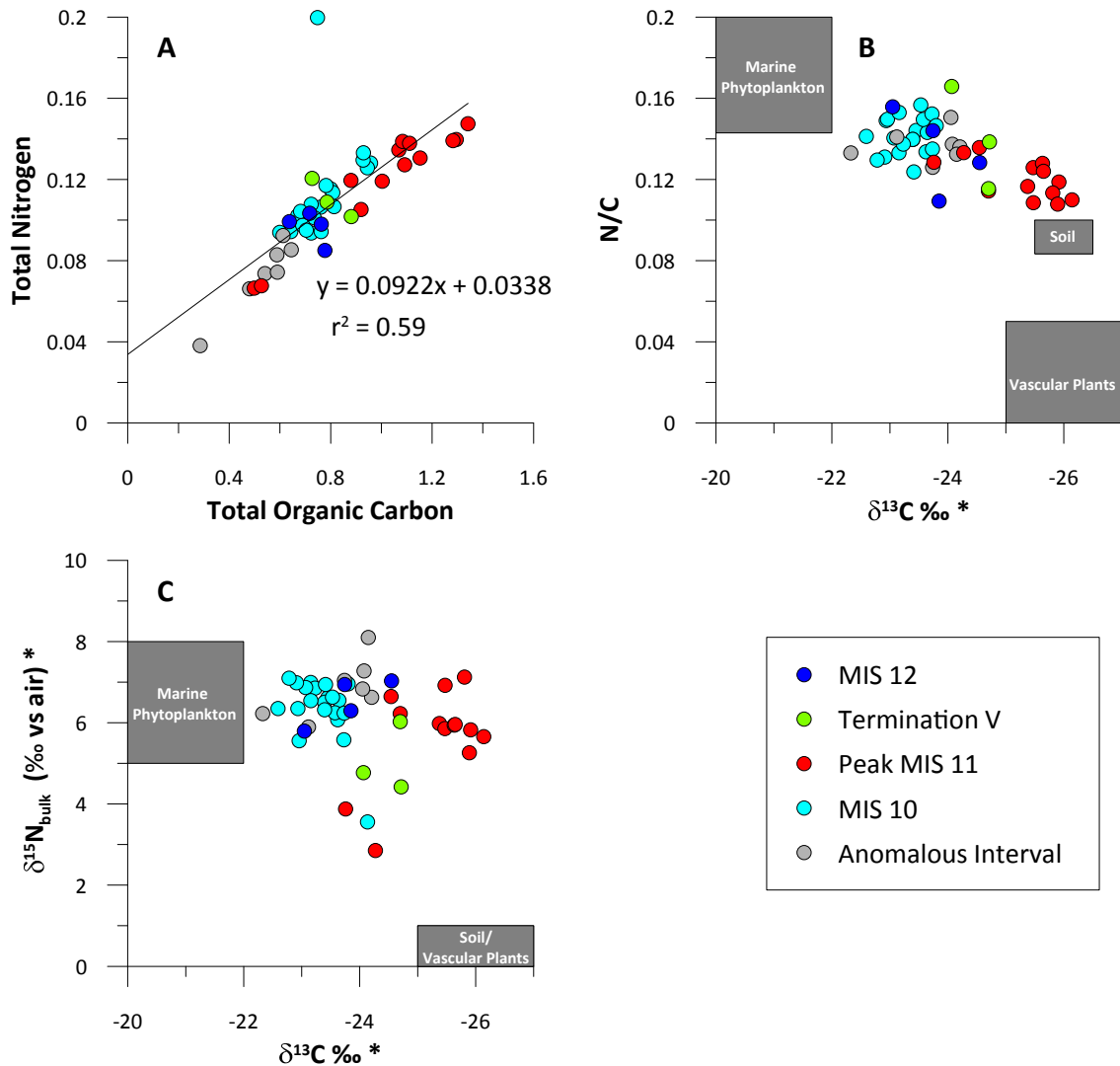


Figure 8. Crossplots of **A.** total nitrogen vs. total organic carbon, **B.** N/C_{rg} vs. $\delta^{13}\text{C}$, and **C.** $\delta^{15}\text{N}$ vs. $\delta^{13}\text{C}$. For each panel, the range of composition of each organic matter source is plotted in a grey box: marine phytoplankton (C/N : 5-7 (Redfield, 1963; Meyers, 1994); $\delta^{13}\text{C}$: -19‰ to -22‰ (Schubert and Calvert, 2001); $\delta^{15}\text{N}$: 5‰ to 8‰ (Walinsky et al., 2009)); Soil (C/N : 10-12, $\delta^{13}\text{C}$: -25.5‰ to -26.5‰, $\delta^{15}\text{N}$: 0‰ to 1‰ (Walinsky et al., 2009)); C_3 vascular plants (C/N : > 20 (Redfield, 1963; Meyers, 1994); $\delta^{13}\text{C}$: -25‰ to -27‰ (Schubert and Calvert, 2001); $\delta^{15}\text{N}$: 0‰ to 1‰ (Walinsky et al., 2009)).

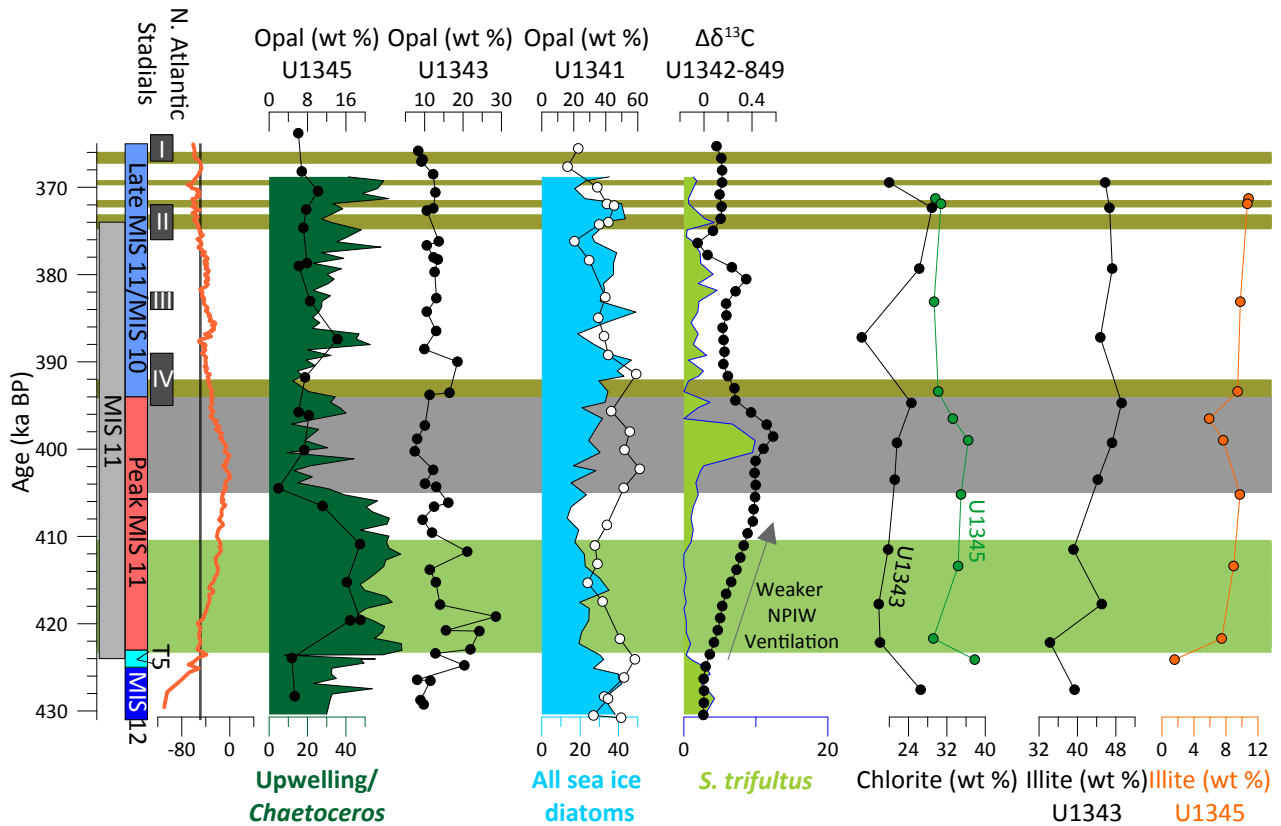


Figure 9. Comparison of Site U1345 with other Bering Sea (U1340, U1341, U1343) and global sites. The grey vertical bar depicts the duration of MIS 11, colored vertical bars refer to the zones mentioned in the text, and dark grey bars show the timing of North Atlantic stadials (I-IV) (Voelker et al., 2010). Global eustatic sea level (orange) is plotted for reference (Rohling et al., 2010). The sill depth of Bering Strait (-50 m amsl) is shown as a vertical grey line. Weight % opal from Sites U1345, U1343, and U1341 (Kanematsu et al., 2013) is plotted with *Chaetoceros* RS relative percent abundances, and relative percent abundances of all sea ice diatoms. The difference in benthic foraminiferal $\delta^{13}\text{C}$ between the Bowers Ridge (U1342) and the North Pacific (ODP 849), a proxy for North Pacific Intermediate Water ventilation, is plotted with relative percent abundances of *Shionodiscus trifultus*, an indicator of highly stratified water. Note that ventilation increases to the left. The weight percent of the clay minerals, chlorite and illite are plotted for Sites U1343 (Kim et al., 2015) and U1345 (this study). Type I Laminations are depicted as pale green bars and Type II laminations are depicted as olive green bars. A grey bar indicates the “anomalous interval.”

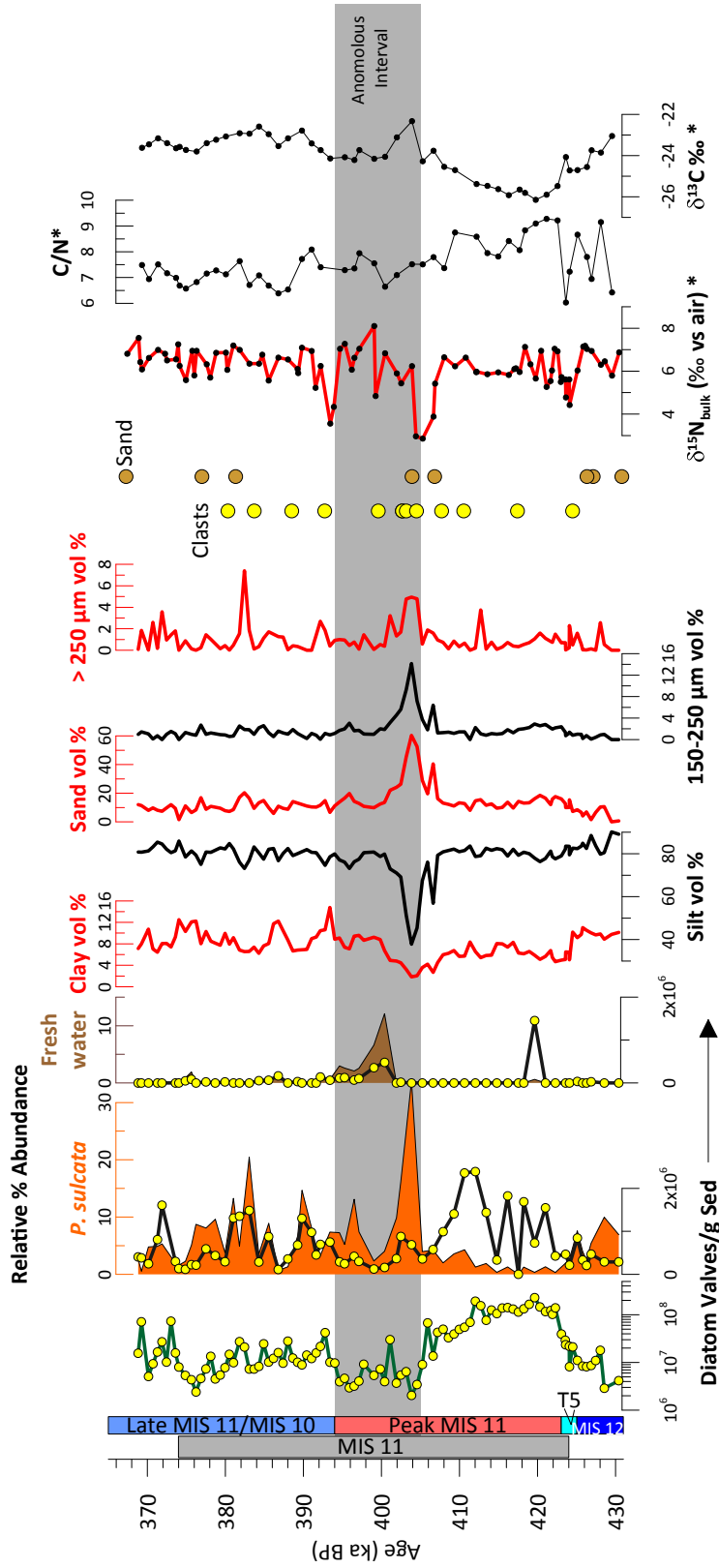


Figure 10. Proxy indicators of shelf to basin transport. The grey vertical bar depicts the duration of MIS 11, colored vertical bars refer to the zones mentioned in the text. Total diatom absolute abundances are plotted next to absolute (line plots) and relative percent abundance of *P. sulcata* (orange area plot) and fresh water species (brown area plot). High-resolution grain size includes % clay, sand, and greater than 250 μm (red lines) and % silt and 150-250 μm (black lines). High-resolution indicate isolated clasts (IRD), maroon circles indicate sand layers for all holes at U1345. Geochemical data is plotted as $\delta^{15}\text{N}$ (red), C/N^* (black), and $\delta^{13}\text{C}$ (black). The grey bar spans 405-394 ka, the so-called, “anomalous interval.”